NASA CONTRACTOR
REPORT

NASA CR-403

NASA CR-40

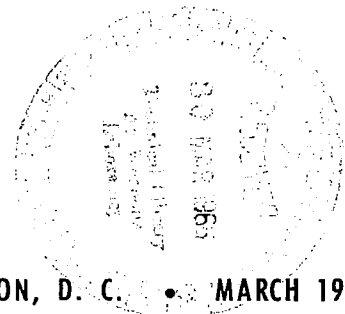# THERMAL CONDUCTIVITY OF HYDROGEN FROM 2000° TO 4700° F

by S. L. Israel, T. D. Hawkins, and S. C. Hyman

NATIONAL AERONAUTICS AND SPACE ADMINISTRATION   •   WASHINGTON, D. C.   •   MARCH 1966

NASA CR-403

THERMAL CONDUCTIVITY OF HYDROGEN

FROM 2000° TO 4700° F

By S. L. Israel, T. D. Hawkins, and S. C. Hyman

FOREWORD

A number of theoretical calculations of hydrogen thermal con-
ductivity at high temperatures have been published, many of which
are in disagreement, especially in the region of dissociation. Until
this investigation, no experimental data existed for equilibrium
dissociated hydrogen. The experimental data used to determine
these properties are recorded in NASA CR-54429. This work was
completed under the technical management of Maynard F. Taylor,
Lewis Research Center, Cleveland, Ohio.

TABLE OF CONTENTS

1. SUMMARY

The thermal conductivity of hydrogen was determined indirectly from measured effective thermal conductivities of porous tungsten specimens in a pressurized hydrogen atmosphere. Measurements were made at pressures of 150, 100, 50, and 15 psia and at temperatures to 4700°F. A truncated-sphere model was used to relate the gas and solid heat transfer contributions in the porous structure. From the model, a relationship is derived which permits determination of the hydrogen thermal conductivity from the measured effective conductivity of the hydrogen-filled porous tungsten specimens when the particle contact area is specified. The particle contact area for each specimen was determined from its measured effective conductivity in vacuum.

The effective thermal conductivity of the hydrogen-filled porous tungsten structure was determined from temperature measurements on the upper circular surface of the right circular cylindrical specimens heated by radio-frequency (r-f) induction currents. A numerical analysis of this boundary value problem was used to relate the measured surface temperature distribution to the axial temperature gradient at the center of the top surface. This axial temperature gradient was used to calculate the effective conductivity of the specimen by equating the heat flux at the center of the top surface to the radiation and natural convection losses at the same point.

The thermal conductivity of hydrogen, determined by the above method, compares reasonably well with previous experimental measurements which extend only to ~3000°F. At low temperatures (below 3500°F) the thermal conductivity is independent of pressure over the range of pressures examined. At high temperatures there is a significant variation in the values of thermal conductivity at different pressures because of dissociation effects. Generally, more dissociation occurs at lower pressures, therefore the thermal conductivities are higher. This trend is in agreement with the theoretical predictions. However, the measured thermal conductivities are higher than those predicted by the theory at temperatures from 3000 to 4700° F. These higher values may be the result of a catalytic action from tungsten on the dissociation of hydrogen in this temperature range. The magnitude of any such effect, however, is not known at this time.

2. INTRODUCTION

2.1 BACKGROUND AND PURPOSE OF INVESTIGATION

Considerable work has been done recently on designing nuclear rockets and other devices which use hydrogen as a coolant or propulsive fluid at high temperatures. This work has led to a need for reliable data on the transport properties, including the thermal conductivity, of hydrogen gas at temperatures in the vicinity of 5000°F. Previously available experimental data on the thermal conductivity extend up to 3000°F. Theoretical calculations[1] based on intermolecular properties indicate that at higher temperatures the thermal conductivity of hydrogen rises steeply with temperature, and is strongly dependent on pressure, even at pressures above one atmosphere.

The purpose of the present investigation was to measure the thermal conductivity of hydrogen at temperatures up to 5000°F and pressures up to 150 psia. These measurements provide independent data for the value of hydrogen thermal conductivity in the range 2000 to 5000°F, and provide a comparison with the predicted strong increase at temperatures above 3000°F.

2.2 PROBLEMS IN MEASURING THERMAL CONDUCTIVITIES OF GASES AT HIGH TEMPERATURES

The usual method of measuring the thermal conductivity of a gas is to measure the temperature drop through a plane or annular layer of the gas with a known heat flux through the layer. In this method, two principal sources of error exist:

3

1. Radiation from solid surface to solid surface across the gas layer

2. Convection of the gas within the layer.

Both of these effects increase the heat flux through a layer with a given temperature drop. At low temperature levels, the radiative heat flux is usually small in comparison with the conductive heat flux, so that an approximate correction for radiation allows good accuracy in determining the conductive heat flux. The effect of convection also may be minimized by keeping the temperature difference small and by employing baffles.

At high temperatures, radiation becomes dominant, and small errors in correcting for this effect may cause large relative errors in determining the conductive heat flux. Also, it is more difficult to maintain small temperature differences at high temperature levels, leading to increased errors due to convection. In addition to these effects, problems involving thermal expansion and mechanical strength of the enclosing structure become important.

Therefore, reliable measurement of the thermal conductivity of a gas at temperatures above 3000°F requires the use of a new experimental method.

2.3 APPROACH TAKEN IN PRESENT PROGRAM

The approach taken in this program is to determine the thermal conductivity of hydrogen gas indirectly from the measured effective or apparent thermal conductivity of a porous tungsten body filled with hydrogen at the desired temperature and pressure. An analytical model of the structure of the porous body and the various modes of internal heat transfer, in conjunction with the measured effective conductivity of the porous body in vacuum, is used to determine the thermal conductivity of the hydrogen from the measurements on the gas-filled body.

The small scale of the porous structure (initial particle size 0.006 to 0.010 in.) serves to minimize both radiation and convection within the gas-filled body,

4

while still being large compared with the mean free path in the gas at an oper-
ating pressure of 150 psia.

Structural problems at high temperatures are eliminated by freely supporting the
cylindrical test specimen and heating it with r-f induction currents. No direct
contact with the specimen by heating or temperature measuring apparatus is
required.

In this method, developed by Hoch[2] for measuring the thermal conductivity of a
solid at high temperatures, the specimen is allowed to radiate freely from its
end surfaces. Temperature observations on only one surface by means of an
optical pyrometer, together with appropriate mathematical analysis, are required
to determine the effective conductivity of the specimen.

The determination of the thermal conductivity of hydrogen from the effective con-
ductivity of the gas-filled specimen is based on the analysis of the modes of heat
transfer in a gas-filled porous body, and the use of an analytical model of the
particle shape and arrangement.

The analysis of heat transfer in the porous body, the method of measuring thermal
conductivities, and the experimental apparatus are described in Section 3. The
analysis of the data and the results are presented and discussed in Section 4.

5

3. TECHNICAL APPROACH

3.1 GENERAL DISCUSSION

The experimental procedure of the present program yields values for the apparent or effective thermal conductivity of the porous tungsten-hydrogen combination. In order to determine the thermal conductivity of the gas, an analysis is required to relate the effective conductivity of the solid-gas combination to the individual conductivities of the solid and gas components.

The development of such an analysis requires an understanding of the various characteristics of a porous structure and their effects on the different mechanisms of heat transfer within the gas-filled porous body. Once this understanding has been achieved, it is then possible to develop a simplified physical model of the porous structure, which will include the important heat-transfer mechanisms in their proper relationship and will be amenable to simple mathematical analysis.

3.2 HEAT-TRANSFER CHARACTERISTICS OF GAS-FILLED POROUS BODIES

The various heat-transfer mechanisms in gas-filled porous bodies have been identified and discussed by Yagi and Kunii[3] and by Kunii and Smith,[4] who developed a simplified equivalent physical structure, and a corresponding algebraic expression for the apparent conductivity in terms of porous-structure parameters and the conductivities of the solid and gas phases. The following heat-transfer mechanisms, shown schematically in Fig. 1, exist in a porous body filled with a stagnant gas:

6

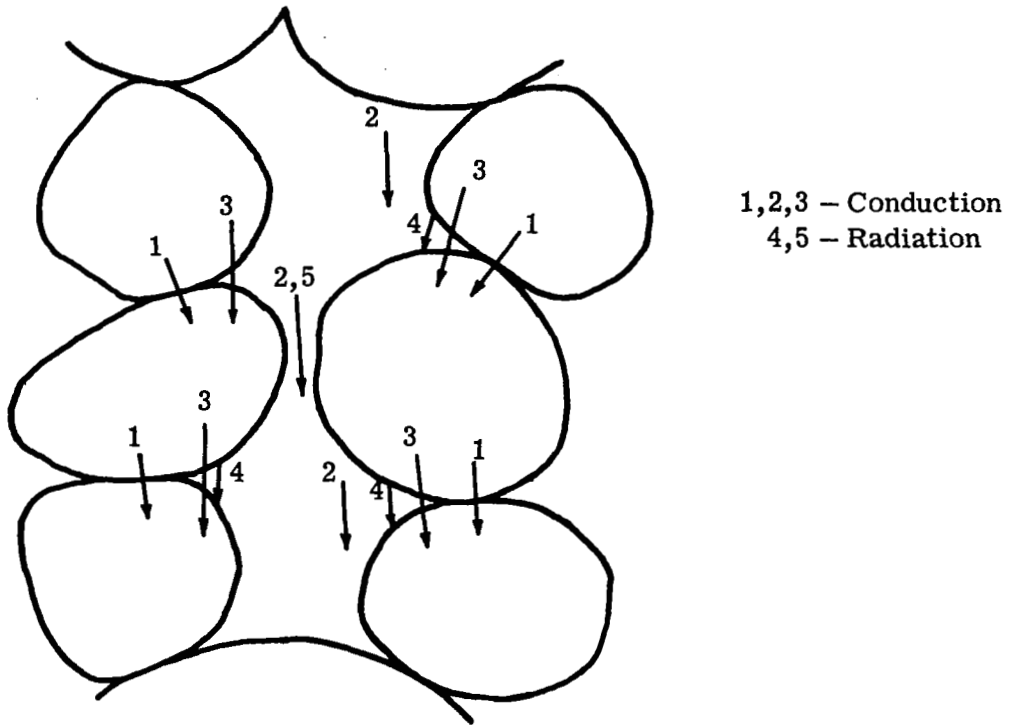1,2,3 — Conduction
4,5 — Radiation

Fig. 1 — Heat Transfer Mechanisms in a Gas-Filled Porous Body

1. Direct solid conduction through areas of actual particle-to-particle contact

2. Direct gas conduction through areas of pore-to-pore communication

3. Series conduction through solid and gas

4. Particle-to-particle radiation across a gas layer

5. Pore-to-pore radiation bypassing the particles.

Of these mechanisms, 1, 2, 3, and 5 may be considered to be in parallel, and 4 to be in parallel with the gas part of 3. Once these heat-transfer mechanisms have been identified and their relationships noted, it is possible to formulate a simplified physical model of a gas-filled porous body and its resulting heat-transfer properties. In this model, the three-dimensional heat transfer within the porous body is reduced to a number of one-dimensional paths, as shown schematically in Fig. 2. Although the model and the resulting general heat-transfer equation are one-dimensional, the three-dimensional geometry of the solid particles is accounted for in determining the relative widths a, δ, and $1-a-\delta$ of the parallel paths and the relative thicknesses ℓ_s and ℓ_g of the layers in series.

The equation for the effective conductivity of this simplified model is

$$k_e = \delta k_s + a k_g + \cfrac{1 - a - \delta}{\cfrac{\ell_s}{\ell k_s} + \cfrac{1}{\cfrac{\ell k_g}{\ell_g} + \ell h_{rs}}} + a \ell h_{rp}$$

in which the radiation effects have been expressed in terms of equivalent heat-transfer coefficients h_{rs} for surface-to-surface radiation and h_{rp} for pore-to-pore radiation.

In the above equation, the first term represents the solid conduction, the second term the gas conduction, the third term the combined effects of series conduction and particle-to-particle radiation, and the fourth term the pore-to-pore radiation.

MIRROR FOR HORIZ. VIEWING

QUARTZ VIEW PORT

COOLING COILS

STAINLESS ST'L. BELL JAR

HIGH FREQUENCY INDUCTION COIL (GENERATOR NOT SHOWN)

TEST SPECIMEN

QUARTZ VIEW PORT

TO VENT THRU FLAME ARRESTOR

FI-1

RD-1

V-5

BACK PRESS. RESTR'N.

PR-1

PRESS. REG.

V-1

V-2

PR-2

PRESS. REG.

HYDROGEN

INERT GAS

GAS PURIFIER

DRYING COLUMN

V-3

ISOLATION VALVES

V-4

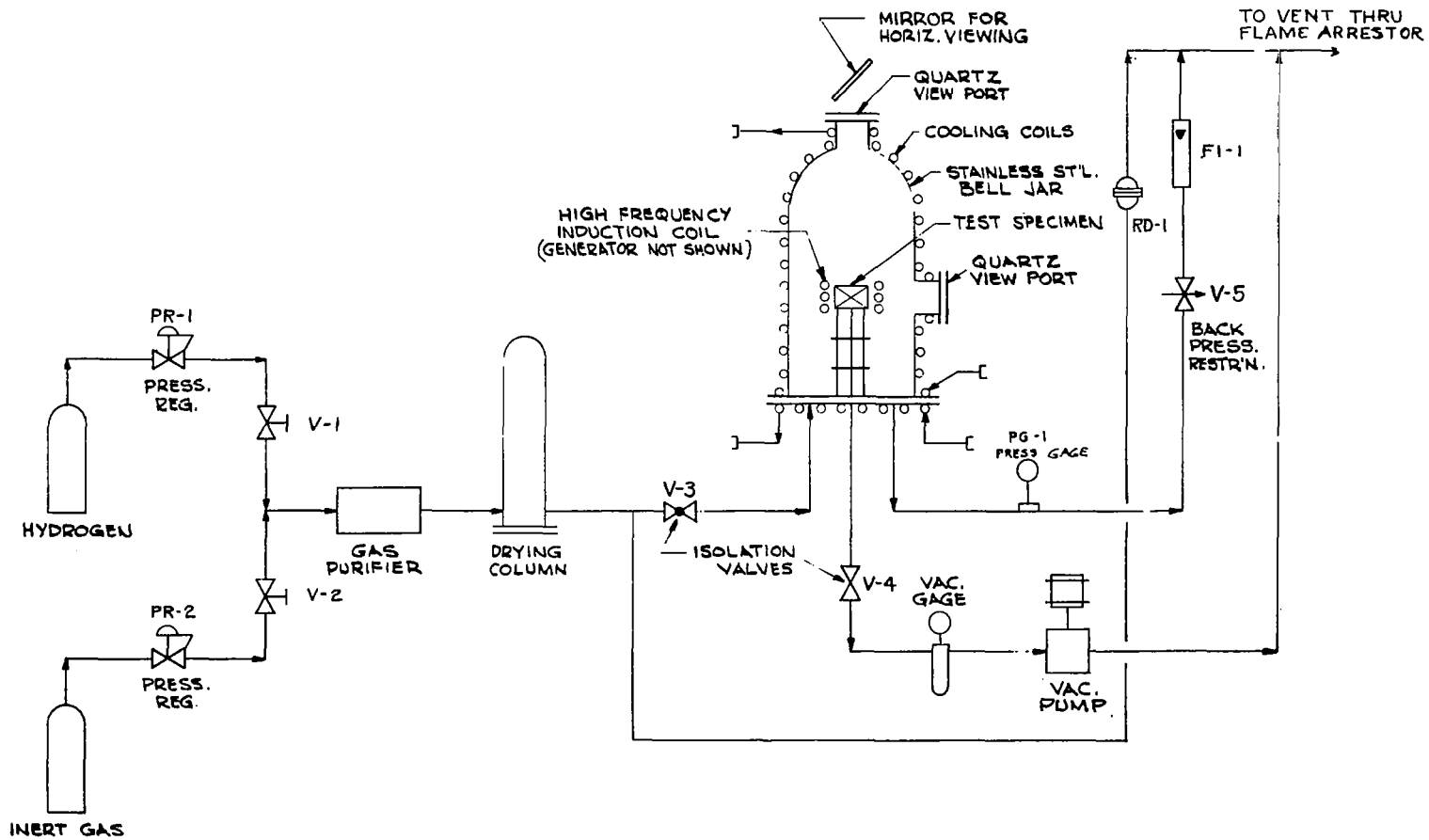**VAC. GAGE**

PG-1 PRESS GAGE

VAC. PUMP

Fig. 2 — Thermal Conductivity Apparatus — Schematic

It is convenient to write the equation in dimensionless form and to define $\varphi_g = \ell_g / \ell$ to yield

$$\frac{k_e}{k_s} = \delta + a\,\frac{k_g}{k_s} + \frac{1 - a - \delta}{(1 - \varphi_g) + \dfrac{1}{\dfrac{1}{\varphi_g}\dfrac{k_g}{k_s} + \dfrac{\ell h_{rs}}{k_s}}} + a\,\frac{\ell h_{rp}}{k_s} \tag{1}$$

This equation helps in understanding the combined heat-transfer properties of a gas-filled porous body in several ways:

1. It shows the direct effect of solid contact area δ, which is expected to be significant for highly sintered metallic particles

2. It shows the relation of the two radiation terms to the actual conduction terms, in particular, the coupling of the particle-to-particle radiation to conduction through the gas layer

3. By examining the form taken by the equation in vacuum ($k_g = 0$)

$$\frac{k_e}{k_s} = \delta + \frac{1 - a - \delta}{(1 - \varphi_g) + \dfrac{k_s}{\ell h_{rs}}} + a\,\frac{\ell h_{rp}}{k_s}$$

it can be seen that a measurement of the effective conductivity in vacuum at one particular temperature does not distinguish between solid contact and internal radiation. Since the equivalent heat-transfer coefficients for radiation, h_{rs} and h_{rp}, are proportional to the cube of the temperature level, a series of measurements at different temperature levels should determine the importance of the radiation terms.

However, the above general equation does not yield explicit information on the influence of particle shape. The entire effect of conduction in series through solid and gas layers is included in the unknown parameter φ_g, which in general is a

function of the conductivity ratio k_g/k_s; it is a constant only for special particle shapes.

Therefore, the above simplified physical model and the resulting equation are not sufficient to determine the heat-transfer characteristics of a gas-filled porous solid. Additional information is needed, either in the form of a calibration with a gas of known conductivity, or in the form of knowledge of the actual particle shape. Of course, a complete description of particle shapes in a real porous solid is not practicable. However, a reasonable approximation to an average particle shape should be sufficient to predict the over-all heat-transfer characteristics of the body.

3.3 PREVIOUSLY USED MODELS OF POROUS STRUCTURES

Several investigators have successfully used simplified models of particle shapes to predict the effective conductivity of gas-filled porous solids. Deissler and Eian[5] considered two specific geometries:

1. Spheres in cubic array (porosity 0.475)
2. Right circular cylinders in square array (porosity 0.215).

The effective conductivities of these two geometries were calculated by means of simple integrations, based on the assumption that the local heat flux is everywhere parallel to the direction of the over-all temperature gradient (zero lateral conductivity). These results, and those for the two limiting cases of all solid and all gas, were then cross-plotted and interpolated to yield predicted effective conductivities for the entire range of porosity (0 to 1), without reference to a specific geometrical structure at intermediate values of porosity.

The predicted values of effective conductivity were then compared with measured values for a compacted powder filled with various gases. The agreement between theory and experiment was reasonably good. Because the material had a porosity

of 0.42, the agreement appears to be principally a justification of the spherical model (porosity 0.475) rather than of the entire analysis.

Gorring and Churchill[6] performed a similar analysis in which a variable parameter in the description of the particle shape allowed adjustment of the porosity. The particle shape assumed was a body of revolution bounded by a cubic curve. The variable parameter allowed finite contact, point contact, or a gap in the lateral direction, but, in the direction of heat transfer, point contact was always assumed. The results of this analysis were also tested against experiments with a variety of gas-filled porous materials. Agreement was generally good except for sintered metallic materials.

Previous work shows that simplified geometrical models of particle shapes have been successful in predicting the conduction heat transfer properties of gas-filled porous materials. However, the analyses described do not treat either solid-contact or radiation effects, which must be considered separately.

3.4 TRUNCATED-SPHERE MODEL

Photomicrographs were obtained of the particle structure of a typical porous specimen. The specimen was vacuum filled with copper to maintain specimen integrity during polishing. The copper was melted out of the pores prior to the taking of pictures of the polished and etched surface. A representative picture is shown in Fig. 3. Examination of the pictures shows that the structure is composed of randomly distributed particles and pores. These pictures do not provide a positive basis for establishing a physical model to represent the porous structure. However, previous investigations have shown that simplified, idealized models of particle shapes used to predict the effective thermal conductivity of gas-filled powders result in calculated values which agree reasonably well with measured values.
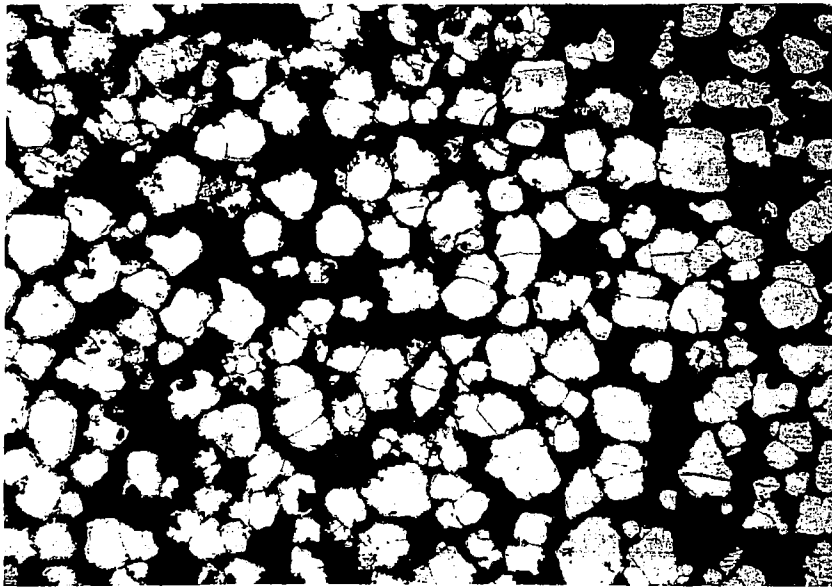
50×

Fig. 3 — Photomicrograph of Porous Structure

A truncated-sphere model was chosen to represent the particle structure of the porous specimens because of the established success of the spherical-particle model in handling the effect of gas conductivity on the important series-conduction mode of heat transfer in gas-filled porous materials. In this model, the local heat flux is assumed to be everywhere parallel, in a direction normal to the particle contact area. Measurements of thermal conductivity of porous tungsten in vacuum show that the results depend on the degree of sintering of adjacent particles. Since the relative size of the contact area is the only adjustable parameter in the model, it is chosen to agree with the measured thermal conductivity of the porous specimen in vacuum. The photomicrographs indicate that a truncated sphere is a reasonable approximation of the particle structure in the contact region. The porosity is not considered directly in the model and any error introduced by not accounting for all of the gas volume is small because of the relatively small contribution of the pore-to-pore gas conduction (mode 2) in the over-all conductivity of the specimen.

The analysis of the effective conductivity of the array of truncated spheres is given in Appendix I (Section 7). As discussed in Reference 7, the data for the porous specimens in vacuum do not show any recognizable effect of radiation with increasing temperatures; therefore, the analysis used includes only the true conduction effects (modes 1, 2, and 3 of Section 3.2). The resulting expression for the effective conductivity is

$$\frac{k_e}{k_s} = \delta + \frac{\pi}{2} \frac{\beta}{(1-\beta)^2} \left[\ln \frac{1}{\beta} - (1-\beta) \right] + \left(1 - \frac{\pi}{4} - \delta \right) \beta \tag{2}$$

where β is the conductivity ratio k_g/k_s. As discussed in the appendix, this expression involves a slight approximation to the geometry of the porous structure. The effect of this approximation is shown to be negligible over the entire range of conductivity ratio β.

When $\beta = 0$ (porous solid in vacuum), Eq. 2 reduces to

$$\frac{k_e}{k_s} = \delta \, .$$

This result agrees with the results of experiments in vacuum; i.e., the effective conductivity of each specimen is a constant fraction of the conductivity of solid tungsten, and no effect of internal radiation is observed. Therefore, for any particular porous specimen, the value of the contact parameter δ can be determined by means of tests in vacuum. Eq. 2 is then an explicit relation between the conductivity ratios k_e/k_s and k_g/k_s for all tests with that specimen in any gas atmosphere.

The derivation of Eq. 2 is equivalent to determining the parameters a and φ_g in Eq. 1, for the special case of no radiation. The values of these parameters for the truncated-sphere model may be obtained, from comparison of Eqs. 1 and 2, as

$$a = 1 - \frac{\pi}{4} - \delta$$

$$\varphi_g = \frac{2\,(1-\beta)}{\ln \dfrac{1}{\beta} - (1-\beta)} - \frac{\beta}{1-\beta}$$

Eq. 2 is plotted in Fig. 4 for values of specimen contact area δ covering the entire possible range from 0 to 1. This figure shows the strong effect of contact area on the effective conductivity of the gas-filled porous solid, and confirms the necessity of using a model which accounts for the contact area.
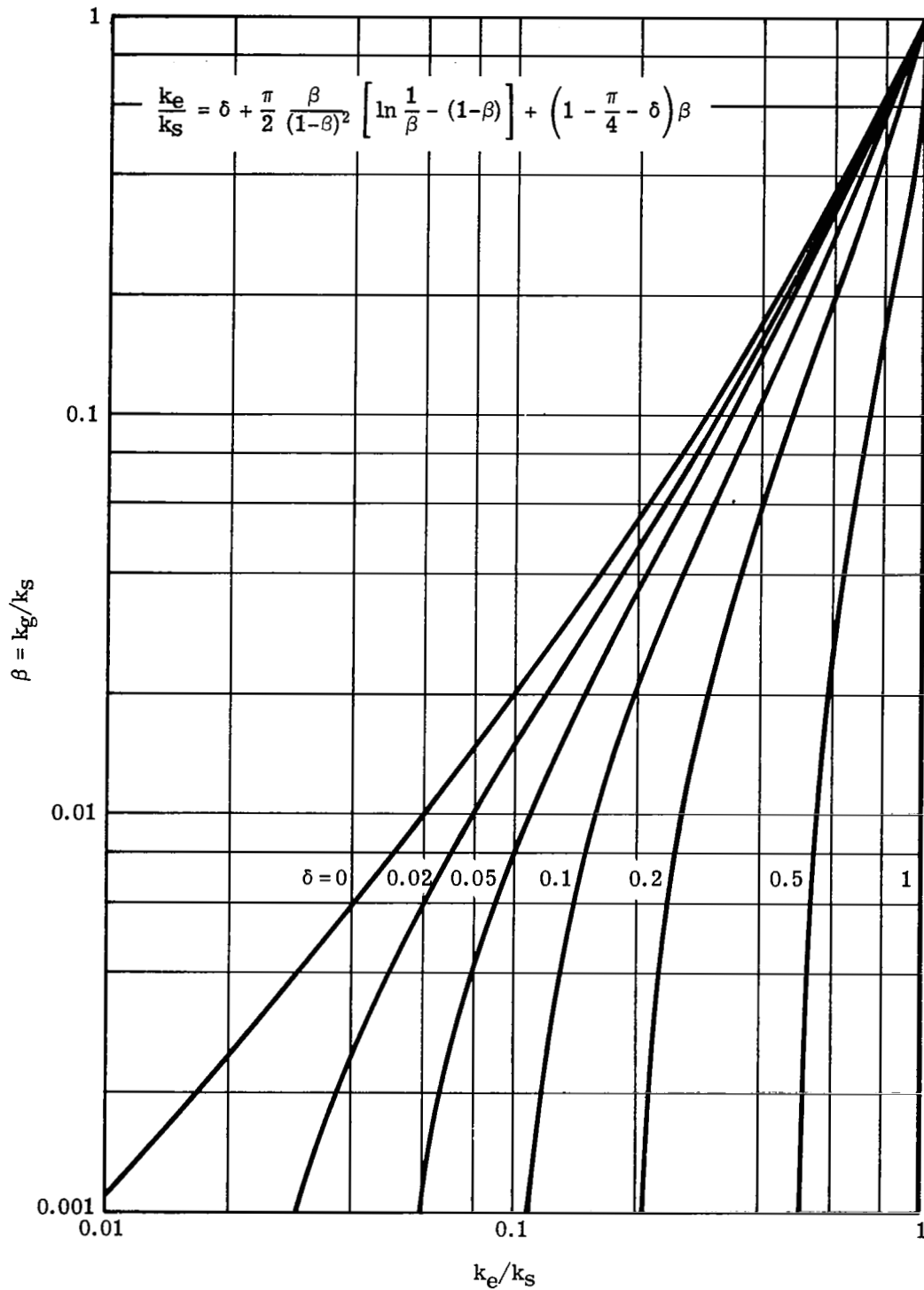
$$\frac{k_e}{k_s} = \delta + \frac{\pi}{2}\frac{\beta}{(1-\beta)^2}\left[\ln\frac{1}{\beta} - (1-\beta)\right] + \left(1 - \frac{\pi}{4} - \delta\right)\beta$$

Fig. 4 — Effective Conductivity for Truncated-Sphere Model

3.5 DETERMINATION OF THE EFFECTIVE CONDUCTIVITY OF THE HYDROGEN-FILLED POROUS TUNGSTEN SPECIMENS

The effective conductivity of the hydrogen-filled porous tungsten specimens is determined from the measured temperature distribution on the upper circular surface of the cylindrical specimens that are heated by r-f induction currents. A cross-sectional view of the arrangement is shown in Fig. 5. Since the heat generation is confined to the outer edge of the specimen, and radiation and natural convection heat losses occur over the entire surface area, a two-dimensional axisymmetric temperature distribution is established in the specimen. A numerical solution to this boundary value problem is used to relate the radial temperature difference on the top surface to the axial temperature gradient at the center of the top surface, as

$$- \left(\frac{\partial T}{\partial z} \right)_{0, L} = \frac{S_0}{R} \; (T_R - T_0) \tag{3}$$

The proportionality factor, S_0, is a function of the specimen geometry. A discussion of this analysis is given in Reference 7 which is the report of a concurrent program to determine tungsten thermal conductivity.

Using the above relationship for the axial temperature gradient, the effective thermal conductivity is determined by equating the heat flux at the center of the top surface to the radiation and natural convection heat losses at that point, as

$$k_e \frac{S_0}{R} \; (T_R - T_0) = \epsilon_T \sigma T_0^4 + Q_{nc} \tag{4}$$

The total hemispherical emittance, ϵ_T, and the natural convection heat flux, Q_{nc}, used in this equation are determined experimentally. The proportionality factor, S_0, is obtained from the analysis in Reference 7. Therefore, the effective conductivity can be determined at different temperature levels from the temperature measurements on the top circular surface of the specimen.

Fig. 5 — Specimen Arrangement
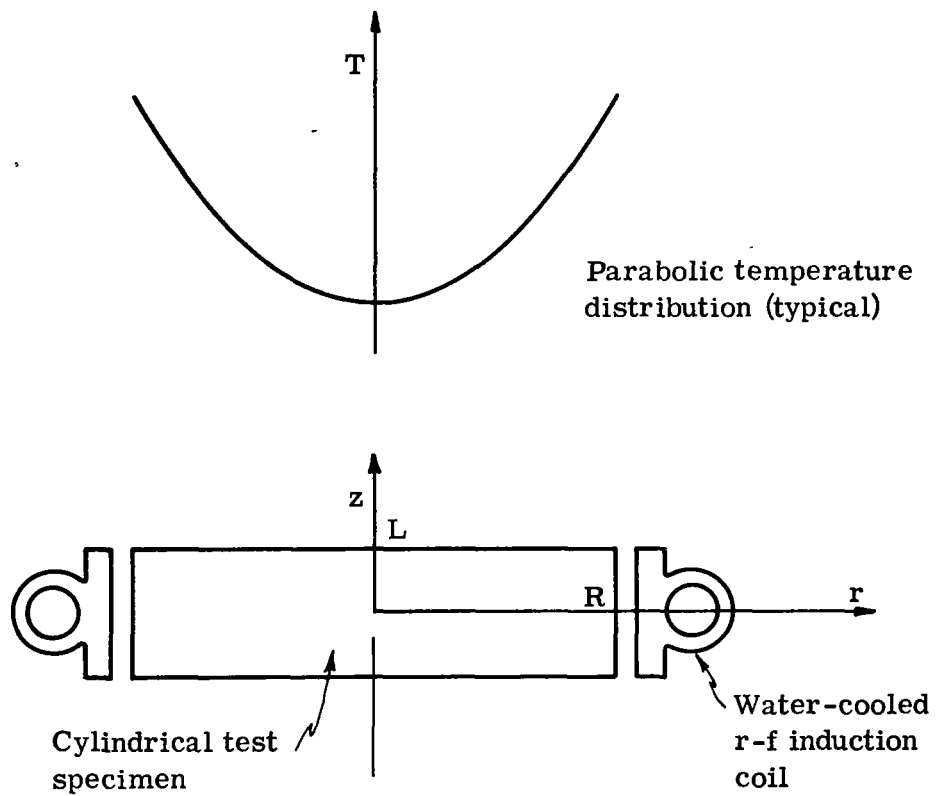
3.6 EXPERIMENTAL APPARATUS

The experimental facility used in the effective conductivity measurements consists of an r-f power unit, a test chamber, atmosphere control, and associated instrumentation. The test chamber is a stainless steel bell jar designed to operate in vacuum or pressurized gas up to 150 psia. The specimen is supported inside the bell jar by a tripod fabricated from tungsten rods. The specimen is centered in a single turn, induction heating load coil. A quartz window, located at the top of the bell jar, permits viewing the upper circular surface of the specimen.

Temperatures are measured with an optical pyrometer using a front surfaced mirror attached to the upper window. The pyrometer is mounted on a circular milling table to permit measurements along perpendicular radii as shown in Fig. 6. The porous specimen has a mottled appearance when viewed through the pyrometer because of the difference in effective emittance between the pores and grains. In all measurements on porous tungsten, the filament in the pyrometer was matched to the pore brightness.

Commercially available bottled hydrogen was used in these experiments. An oxygen removal unit and a gas drier in the flow circuit further purify the gas before it enters the test chamber. The test chamber is vented to the atmosphere through a flame arrester. A Bourdon tube-type pressure gauge is used to measure the test chamber pressure.

A more detailed description of the apparatus is available in Reference 7.
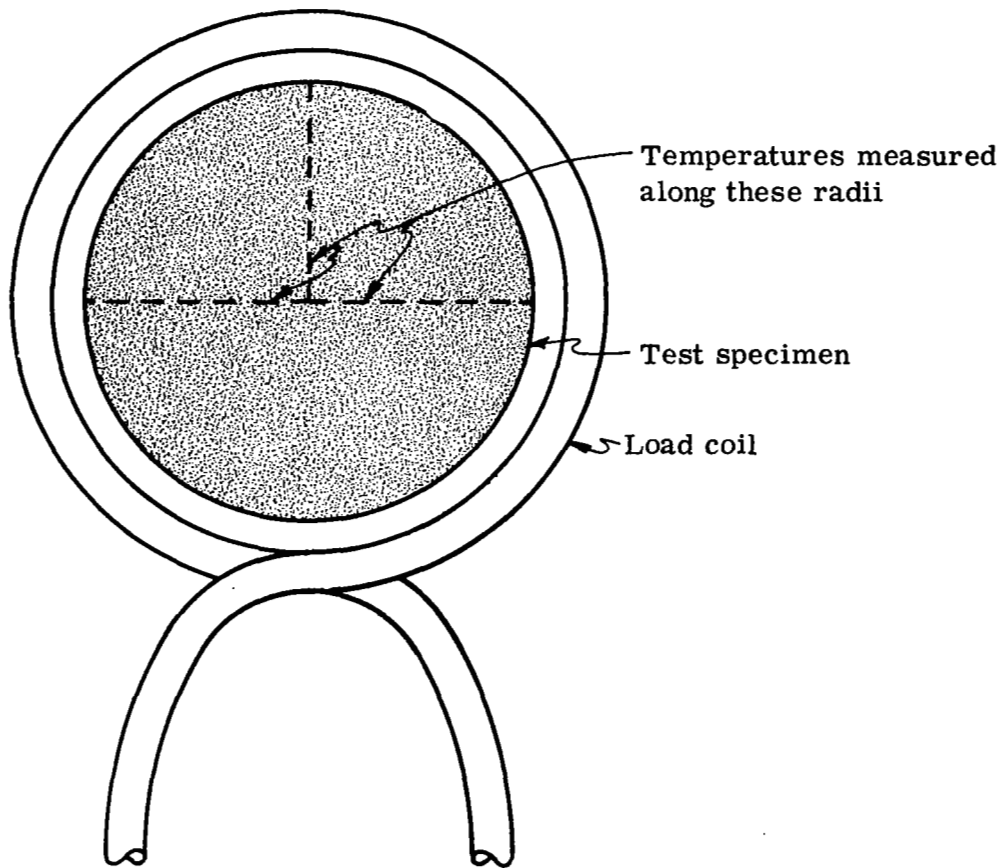
Fig. 6 — Location of Temperature Measurements on Test Specimen

4. HYDROGEN THERMAL CONDUCTIVITY MEASUREMENTS

Hydrogen thermal conductivity measurements were made at temperatures from 2000 to 4700°F and at pressures of 150, 100, 50, and 15 psia. The porous tungsten specimens used in these experiments were fabricated from 0.006 to 0.01-in. particles by gravity sintering at temperatures above 4000°F for a sufficiently long time to insure mechanical stability of the structure. The specimens, listed in Table 1, had porosities of approximately 0.45 except for the sample, trial

TABLE 1 — POROUS TUNGSTEN TEST SPECIMENS

	Diameter, in.	Height, in.
P1	1.52	0.538
P2	1.45	0.507
P3	0.975	0.379
P4	1.03	0.302
P5	0.80	0.25

specimen P1, which had a porosity of approximately 0.55. The particle size used in the specimens represents a compromise between the following conflicting requirements:

1.   The pore size should not be small in comparison with the mean free path of the gas molecules at the operating temperatures and pressures.

2. The dimensions of the structure should be small to reduce temperature differences between adjacent particles and thereby minimize internal radiation.

According to an analysis presented by Deissler and Eian,[5] the first requirement is satisfied at an operating pressure of 150 psia. The thermal conductivity measurements of the porous specimens in vacuum[7] show that the second requirement is satisfied.

In performing the experiments, the system was first evacuated to 10 microns Hg and the specimen was heated to 2300°F to drive off any residual gases. The system was then pressurized and evacuated three times to minimize impurities in the gas atmosphere. Measurements were made at the highest pressure first. The bell jar was then vented to obtain data at the lower pressures.

Specimens were heated at constant power for 20 to 30 minutes to achieve steady-state conditions before making temperature measurements. Two temperature measurements were made at several locations along each of the three radii on the upper surface of the specimen as shown in Fig. 6. A typical set of data is shown in Fig. 7.

A numerical solution to the boundary value problem represented by the induction heated specimen was obtained with the digital computer code discussed in Reference 7. This analysis accounted for the experimentally observed finite depth of heating (0.2 in.) at the outer surface of the porous specimen, and accounted for radiation and natural convection heat losses from the surface. The results showed a peak temperature on the top surface at about 0.1-in. from the outer edge of the specimen. This corresponds to the experimental results. In addition, the computed temperature distribution on the top surface was found to be parabolic in the no heat generation region. This agrees with the data shown in Fig. 7. These results are similar to these obtained for heating a porous specimen in vacuum.[7]
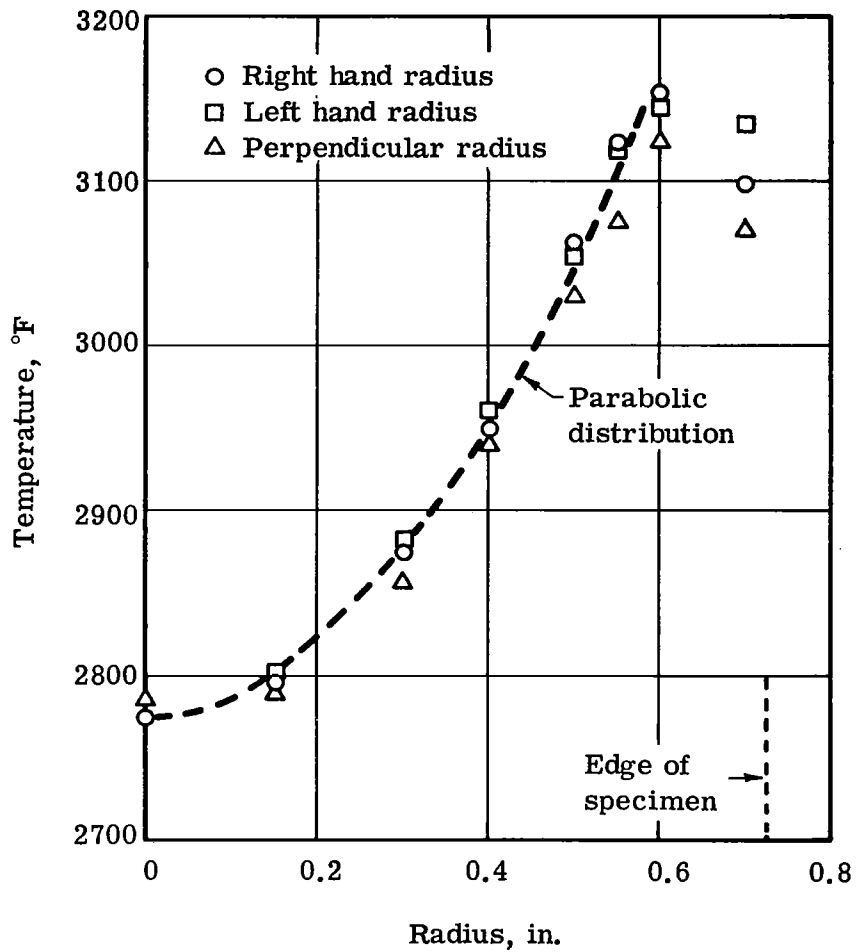
Fig. 7 — Temperature Distribution for $1\frac{1}{2}$-in. Porous Tungsten Specimen in Hydrogen (150 psia)

The expression used to calculate the effective thermal conductivity of the gas-solid specimens is

$$k_e = \frac{\epsilon_T \sigma T_0^4 + Q_{nc}}{\frac{S_0}{R}(T_R - T_0)} \quad . \tag{5}$$

The temperatures used in the above equation were obtained from a least squares parabolic curve fitted to the temperature data. The proportionality factors, S_0, and the total hemispherical emittances for porous tungsten were those determined in Reference 7. The natural convection heat flux was determined experimentally as discussed in Section 5.

The calculated effective thermal conductivities for one of the specimens in hydrogen is shown in Fig. 8. The data show a pronounced increase in effective thermal conductivity values compared to those obtained with the specimen in a vacuum. All specimens showed this effect which demonstrates the heat transfer contribution of the hydrogen to the effective thermal conductivity of the porous structure. The pressure level also significantly affects the effective thermal conductivities of the specimens. The higher pressures result in lower effective thermal conductivity values.

The experimental data and calculated effective thermal conductivities for all specimens are included in Reference 8. These calculated effective thermal conductivities of the gas-filled porous specimens were used to determine the hydrogen thermal conductivity. The analysis of the truncated sphere model, presented in Section 3, results in Eq. 2, relating the gas thermal conductivity to the effective thermal conductivity. For convenience the expression is repeated below, with k_g/k_s substituted for β.
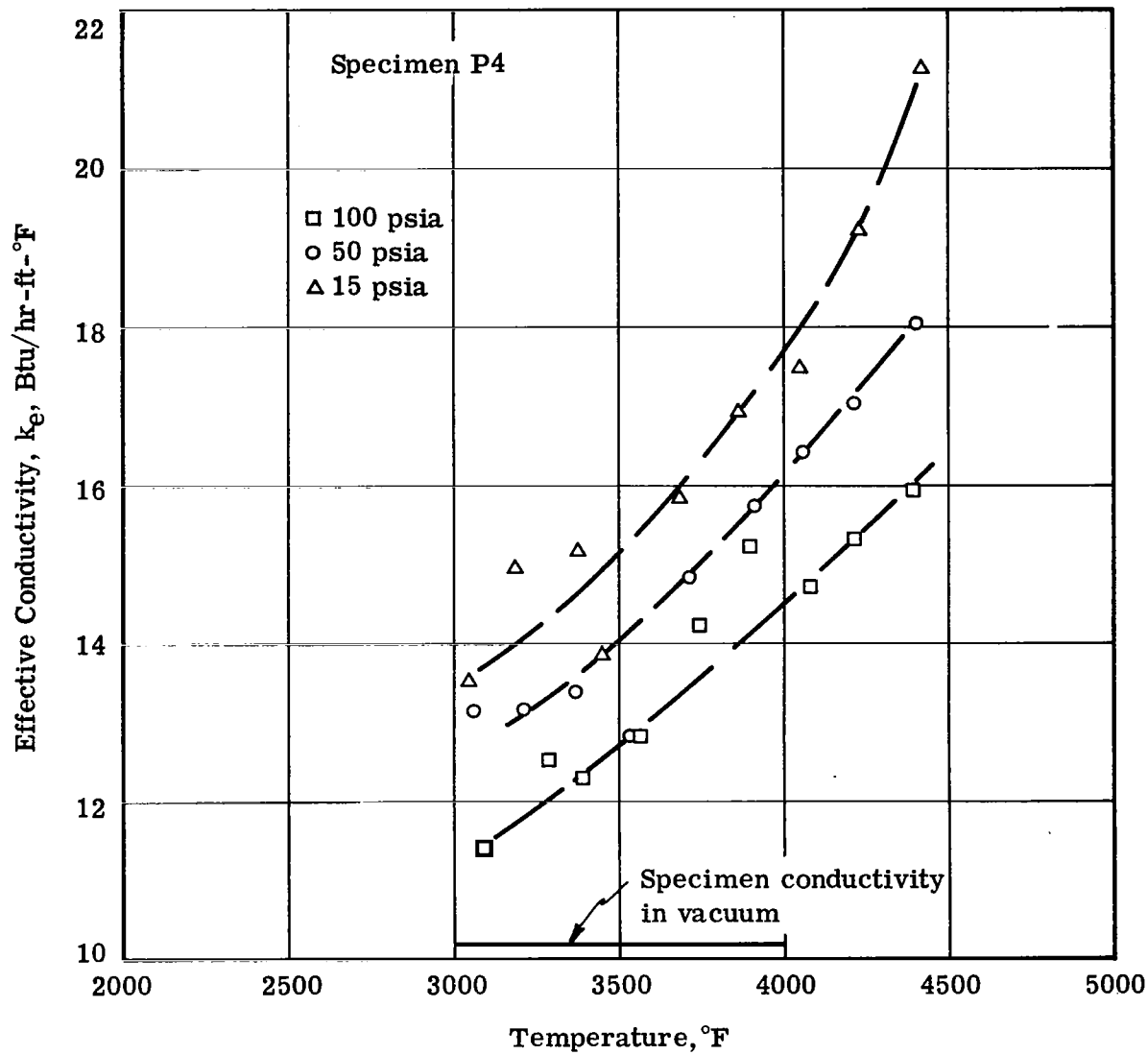
Fig. 8 — Effective Conductivity of Porous Tungsten in Pressurized Hydrogen

$$\frac{k_e}{k_s} = \delta + \frac{\pi}{2} \frac{k_g/k_s}{[1-(k_g/k_s)]^2} \left\{ \ln \frac{1}{k_g/k_s} - [1-(k_g/k_s)] \right\} + (1 - \frac{\pi}{4} - \delta) \times$$
$$\times (k_g/k_s) \qquad (2)$$

In the above expression, δ is the fractional particle contact area which is determined by the ratio of the specimen's thermal conductivity in vacuum to solid tungsten thermal conductivity. These values and the values of solid tungsten thermal conductivity are included in Reference 7. The gas thermal conductivity could not be calculated explicitly from Eq. 2. Consequently, a graphical method using curves similar to those shown in Fig. 4 was used to obtain final values.

Hydrogen thermal conductivities at pressures of 150, 100, 50, and 15 psia are shown in Figs. 9, 10, 11, and 12, respectively. The scatter in the data at the higher pressures resulted from natural convection currents at the specimen surface which introduced some optical distortions during temperature measurements. These distortions are greatly reduced at the lower gas pressures and result in considerably less scatter in the data. There is no demonstrable effect of specimen geometry on the calculated values of hydrogen thermal conductivity; however, the specimens did not produce the same degree of reproducibility of the data at 100 psia that was achieved at the other pressures. No logical explanation of this result has been developed.

Best-fit curves of the data at each pressure are presented in Fig. 13 to show the effect of pressure on the hydrogen thermal conductivity. It is evident that the conductivity is strongly dependent on temperature and pressure above approximately 3500°F. There is a distinct trend of increasing conductivity with decreasing pressure.These trends are in agreement with theoretical predictions of hydrogen thermal conductivity[1] which account for the dissociation of the hydrogen molecule at these temperatures and pressures.
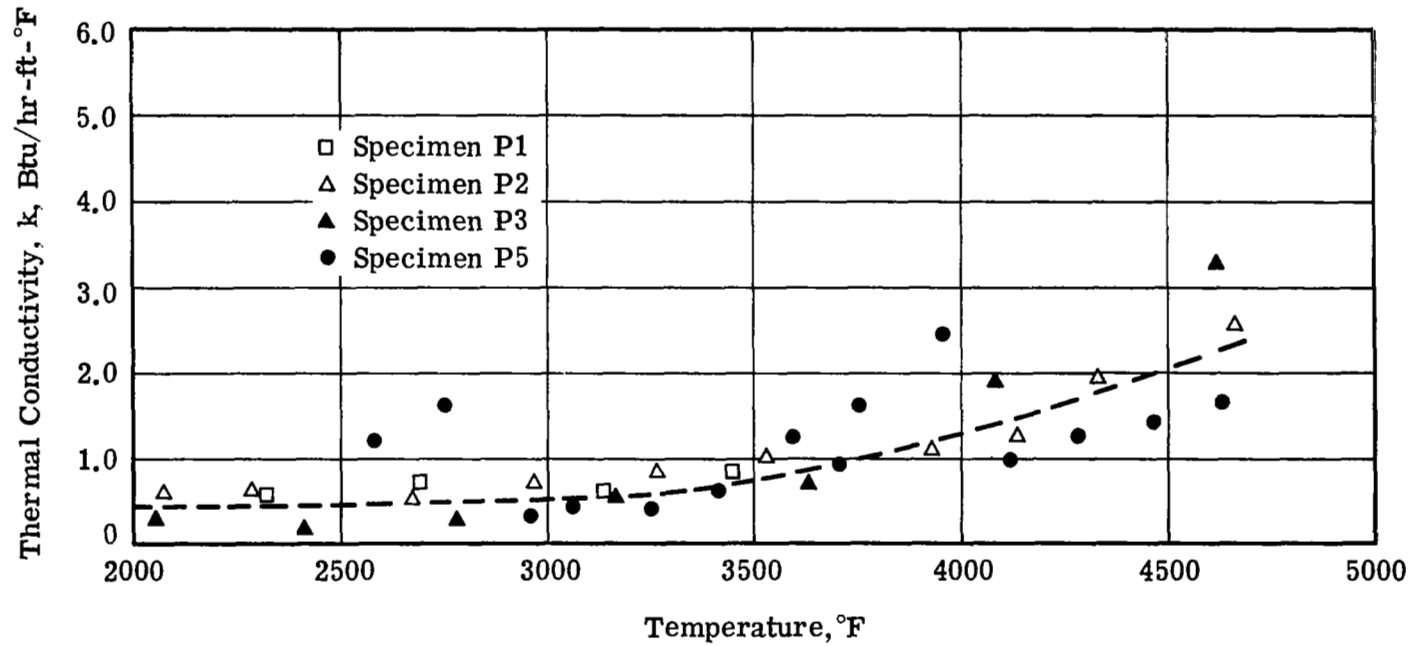
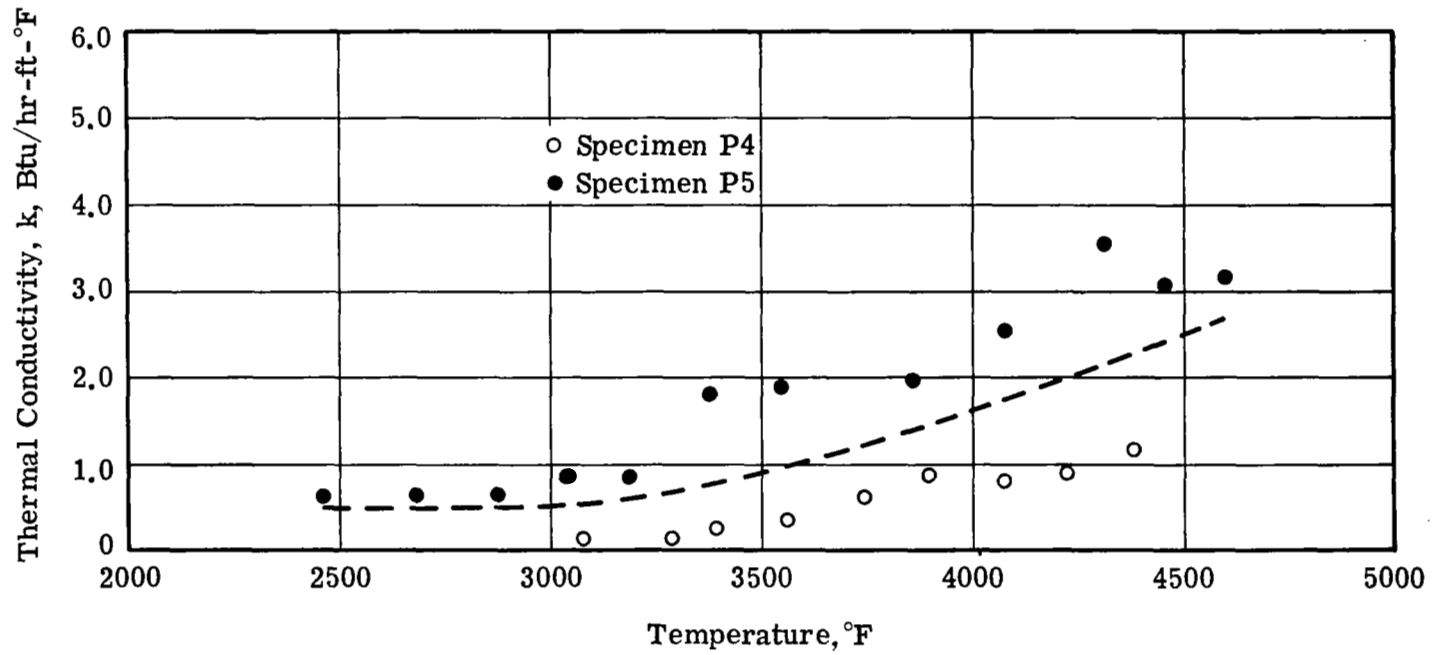Fig. 9 — Hydrogen Thermal Conductivity, 150 psia

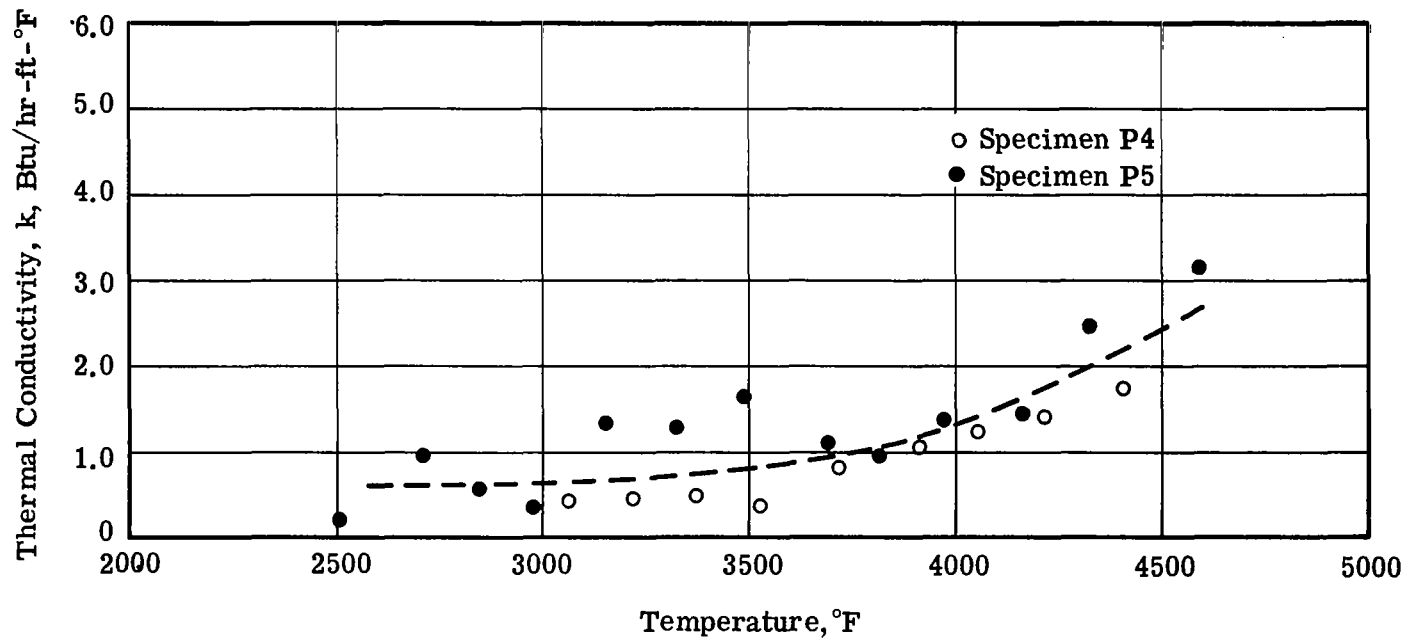Fig. 10 — Hydrogen Thermal Conductivity, 100 psia
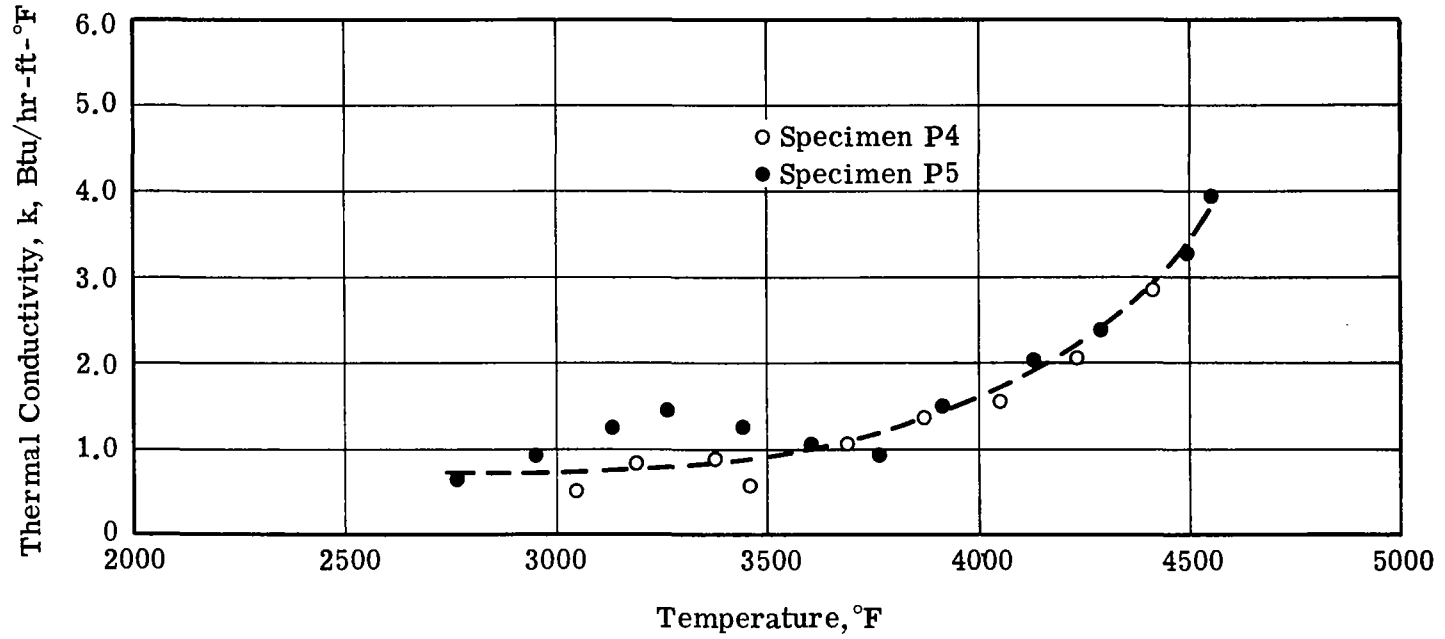
Fig. 11 — Hydrogen Thermal Conductivity, 50 psia

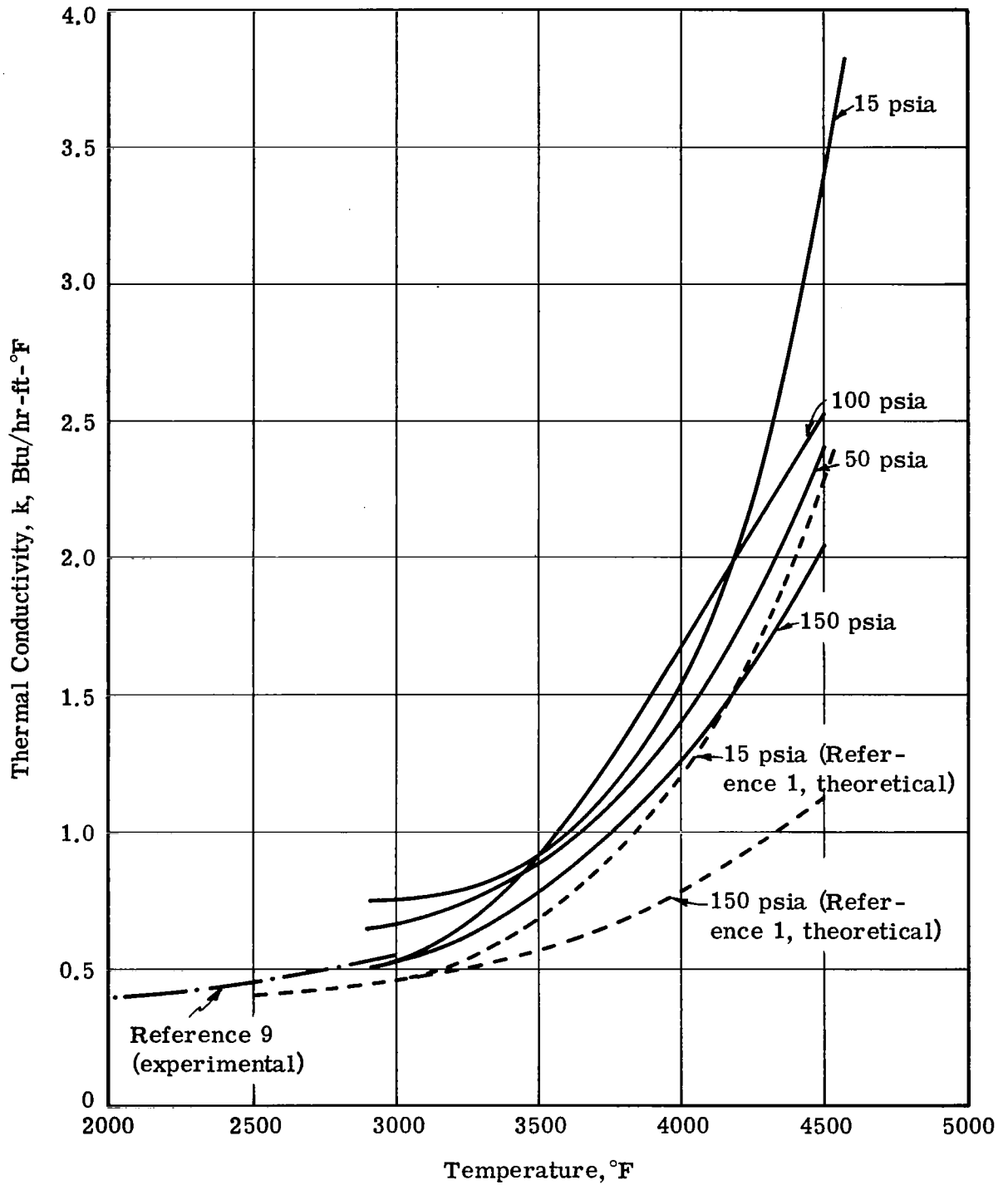Fig. 12 — Hydrogen Thermal Conductivity, 15 psia

Fig. 13 — Hydrogen Thermal Conductivity, Best-Fit Curves

The measured thermal conductivities shown in Fig. 13 are in reasonably good agreement with previous experimental and theoretical results at 3000°F. At higher temperatures, the measured values are higher than the theoretical predictions at 15 and 150 psia. There are no other experimental data available at these temperatures. The largest uncertainty in the calculated values results from uncertainties in experimentally determined natural convection heat fluxes. There is a 50% uncertainty in these measurements. However, the natural convection represents only a portion of the heat loss from the specimen. A 50% uncertainty in its value produces only a 20% uncertainty in the calculated thermal conductivity at 5000°F, a 27% uncertainty at 4000°F, and a 60% uncertainty at 3000°F. Even with these uncertainties taken into account, the measured conductivities are still higher than the theoretical predictions at the higher temperatures. These higher values may be the result of a catalytic action from tungsten on the dissociation of hydrogen in this temperature range. The magnitude of any such effect, however, is not known at this time.

5. HYDROGEN NATURAL CONVECTION MEASUREMENTS

Natural convection heat fluxes applicable to the porous specimens were determined from conductivity measurements of similar solid tungsten specimens in vacuum and pressurized hydrogen atmosphere. The thermal conductivity of solid tungsten, which was determined in a vacuum, is not affected by the presence of hydrogen. However, the hydrogen does contribute to the heat loss from the specimen. The expression for determining the thermal conductivity of solid tungsten in hydrogen is the same as that given for the porous tungsten specimen in Section 3, except that in this case the thermal conductivity is known. Consequently, the hydrogen natural convection heat flux can be determined from the following expression,

$$Q_{nc} = k_S \frac{S_0}{R} (T_R - T_0) - \epsilon_T \sigma T_0^4$$

where k_S is the thermal conductivity of solid tungsten reported in Reference 7.

The four solid specimens used in these experiments are listed in Table 2. The experimental procedure and apparatus are the same as described for the porous tungsten in the preceding sections. Measurements were made at center temperatures between 2000 and 4700°F and at pressures of 150, 100, 50, and 15 psia.

The results of these tests are shown in Fig. 14 for all specimens and pressures. The experimental scatter is such that no separation of the data can be made ac-
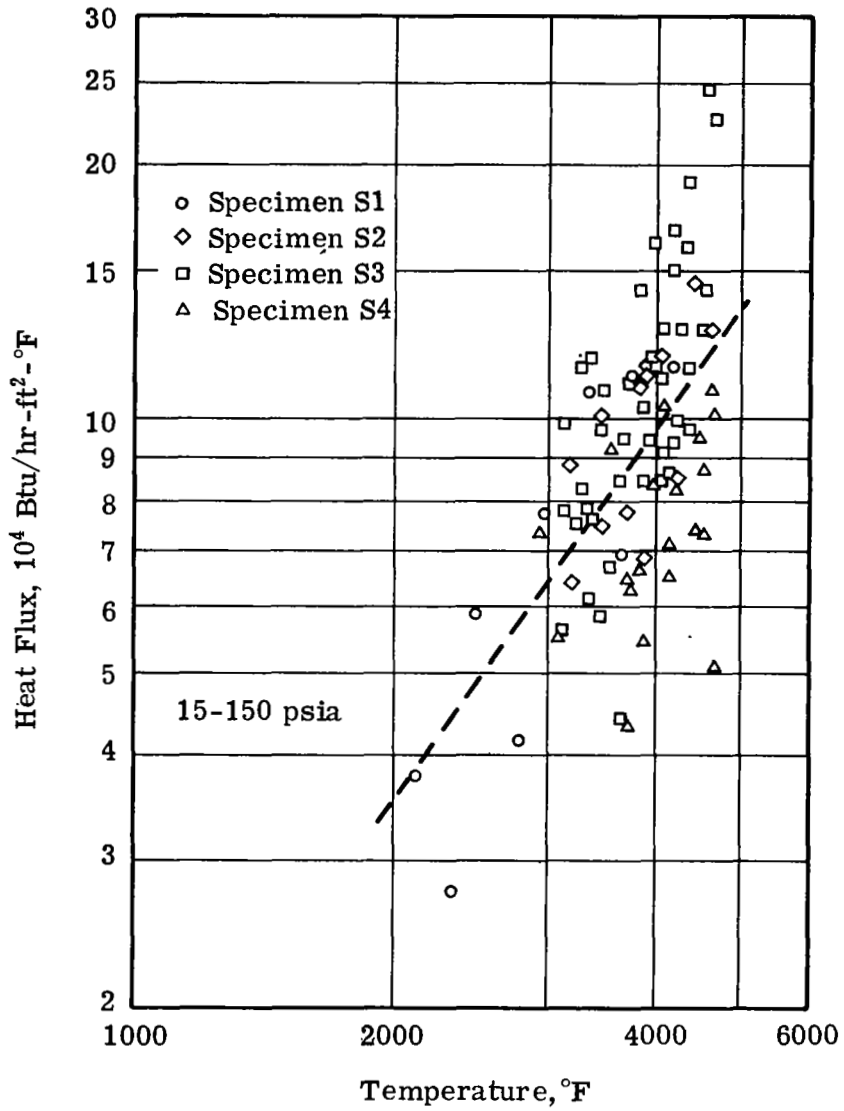
Fig. 14 — Natural Convection Heat Flux for Hydrogen

TABLE 2 — SOLID TUNGSTEN
TEST SPECIMENS

	Diameter, in.	Height, in.
S1	1.52	0.502
S2	1.006	0.504
S3	1.0066	0.356
S4	0.804	0.284

cording to specimen size or pressure level. As a result, the best-fit line shown in Fig. 14 was used for the calculation of all the porous tungsten conductivities at different pressure levels.

These results do not agree with natural convection heat fluxes calculated from the usual empirical correlations using property values at mean temperatures between the bulk and surface. The empirical correlations predict a significant difference in heat fluxes for the different pressure levels, and to a lesser extent, they predict some difference caused by variation in specimen size. Because of the large temperature difference between specimen surface and bulk temperature, the empirical correlation may not be valid (especially for hydrogen, which dissociates at these high temperatures and thus has strongly temperature dependent physical properties).

6. FEASIBILITY OF EXTENDING METHOD TO OTHER GASES

6.1 GENERAL DISCUSSION

Eq. 2, which relates the gas thermal conductivity to the effective thermal conductivity of the test specimen, is a general expression that, theoretically, can be applied to any gas-filled porous solid when there is no significant amount of internal radiation within the porous structure. Experimentally, however, the gas thermal conductivity is required to be sufficiently large to result in measurable increases in the effective thermal conductivity of the gas-filled porous structure compared to the effective thermal conductivity of porous specimens in vacuum. Fig. 8 shows that this requirement is satisfied for the hydrogen-tungsten system used in this investigation. The feasibility of extending this method of thermal conductivity measurement to other gases, therefore, depends in part on selecting appropriate gas-solid material combinations. The materials, of course, must be compatible with the gas atmosphere at the temperatures and pressures of interest.

For gases such as nitrogen and argon, selection of a suitable porous material is limited because of their low thermal conductivities. The thermal conductivity of these gases is approximately an order of magnitude lower than that of hydrogen. Consequently, the porous material must have a proportionately lower effective thermal conductivity to permit measurements of the contribution which the gas makes to the effective thermal conductivity of the porous structure in the gas

atmosphere. Lower effective thermal conductivities of the porous structure can be achieved by two methods:

1. Increase the porosity of the porous structure for a material such as tungsten.

2. Select a lower thermal conductivity solid material from which the porous structure is to be fabricated. In the temperature range of interest (2000 to 5000°F) ceramics are the only suitable materials which have sufficiently low values of thermal conductivities.

Both of these methods introduce significant amounts of internal radiation heat transfer within the porous material at the temperatures of interest. For highly porous tungsten materials this internal radiation is primarily due to scattering and pore-to-pore radiation within the porous structure. For the ceramic materials, some of which become optically transparent at these high temperatures, the internal radiation heat transfer can be by absorption and transmittance through the structure, as well as by scattering. These effects are described more fully in Appendix II.

These radiation heat fluxes and their interaction with the conduction heat fluxes must be considered when calculating the temperature distributions within the specimen, and when relating the gas thermal conductivity to the effective thermal conductivity of the porous specimen. A basic requirement for extending this method to other gases, therefore, is the development of analytical models which adequately account for the internal radiation heat fluxes.

## 6.2 EXPLORATORY EXPERIMENTS WITH A HIGHLY POROUS TUNGSTEN SPECIMEN

To provide preliminary evaluations of internal radiation within highly porous materials having lower effective thermal conductivities, thermal conductivity measurements were made using a tungsten specimen having a porosity of approximately

95%, with a pore size on the order of 0.02 to 0.03 in. The highly porous nature of this "foamed tungsten" material is shown in Fig. 15. Specimen dimensions were 1-in. diameter × 0.3-in. high. Measurements were made in vacuum and in hydrogen and argon atmospheres at 100 psia. Measured effective thermal conductivities under these conditions are shown in Fig. 16. The following qualitative conclusions can be drawn from these data.

1. Effective thermal conductivity values in vacuum show a significant increase with temperature. Values increase by a factor of two over the temperature range of the measurements. Since the thermal conductivity of solid tungsten is not a strong function of temperature in this range, such an increase in the effective thermal conductivity of the specimen can result only from internal radiation heat fluxes.

2. In argon at 100 psia, no measurable contribution to the effective thermal conductivity of the specimen results below 3000°F, and only minor contributions result above this temperature. This indicates a requirement that the test specimen effective thermal conductivity in vacuum must be lower yet for measurements of the thermal conductivities of gases such as argon and nitrogen.

3. Hydrogen at 100 psia contributes substantially to the effective thermal conductivity of the specimen. The internal radiation heat fluxes, however, do not permit the determination of meaningful values of gas thermal conductivity from the present analytical models (which include conduction heat fluxes only).

6.3 EXPLORATORY EXPERIMENTS WITH A CERAMIC TEST SPECIMEN

Consideration of ceramic test specimens introduces the requirement of properly heating a nonconducting material with r-f induction heating equipment. An experiment was conducted to evaluate a variation in the method used to heat the porous

4×

20×
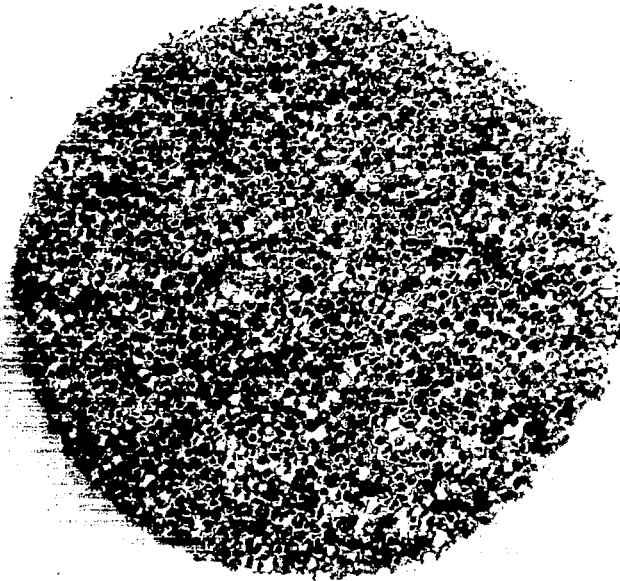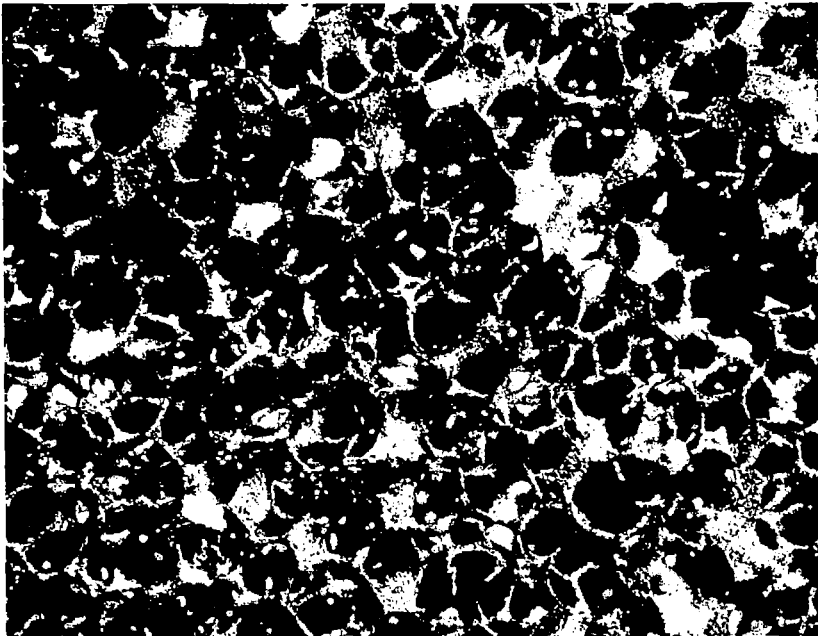
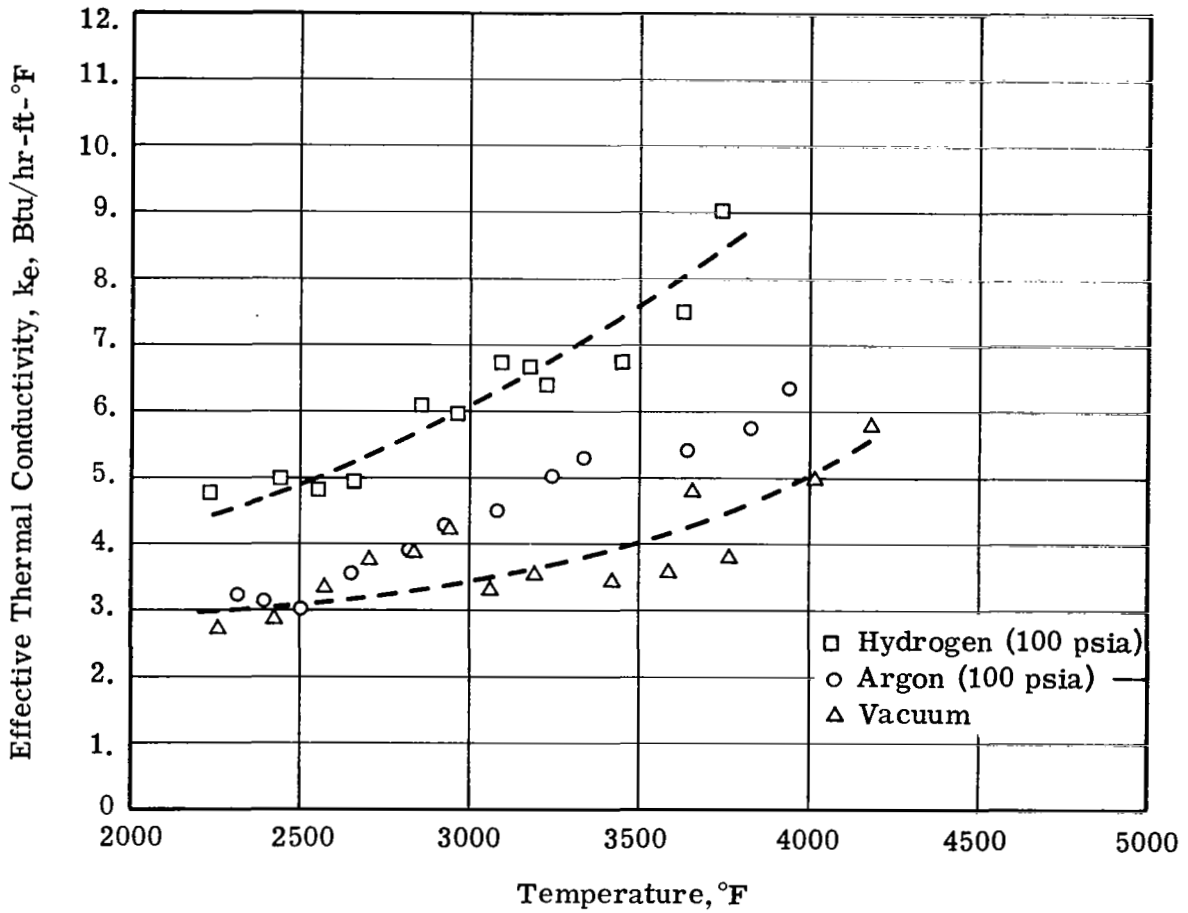Fig. 15 — Photomicrographs of Foamed Tungsten

Fig. 16 — Effective Conductivity of Foamed Tungsten in Vacuum, Hydrogen, and Argon

and solid tungsten specimens. The variation consisted of heating the vertical surface of a cylindrical solid ceramic specimen with a radiating susceptor. The arrangement for heating the specimen is shown in Fig. 17.
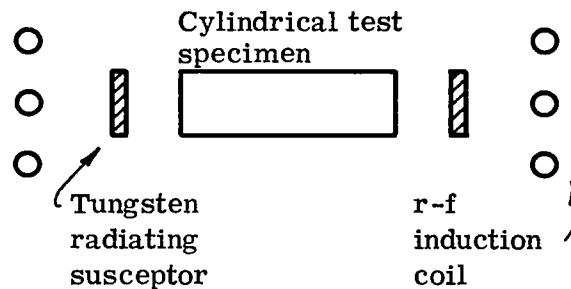
Fig. 17 — Test Setup for Ceramic Specimen

Measurements were made in vacuum at 2300°F. A $1\frac{1}{2}$-in. diameter tungsten cylinder, 0.5 in. long, having a wall thickness approximately 0.040 in., was used as the susceptor. This cylinder was on hand from a previous experiment and did not provide optimal view factors between the susceptor and specimen surfaces.

The test specimen was a high density (5.7 g/cc) zirconia cylinder, 0.75-in. diameter $\times$ 0.375-in. high. The specimen was obtained from the Zirconium Corporation of America and is identified by the trade name Zircoa 1027. Representative thermal properties for this material are:*

1. Total emittance ϵ_T (at 2760°R): 0.27 (extrapolated — no data above 2000°R)
2. Thermal conductivity = 1.6 Btu/hr-ft-°F (corrected for a density of 5.7 g/cc)
3. Spectral emittance ϵ_λ = 0.4.

---

*Taken from WADC-TR-58-476.

The measurement resulted in a value of 1.74 Btu/hr-ft-°F for the thermal conductivity of the specimen, which is in reasonable agreement with the value listed above. Following the measurements, a very thin grayish deposit was observed on the surface of the specimen. What effect this may have had on the emittances of the specimen is difficult to estimate, but it may account for the somewhat higher thermal conductivity value obtained.

6.4 HELIUM THERMAL CONDUCTIVITY MEASUREMENTS

Previous measurements of the thermal conductivity of helium (reported in Reference 9) indicate that at temperatures in the vicinity of 3000°F the values are sufficiently high to permit measurements by the same method used for the hydrogen thermal conductivity determinations. Measurements of helium thermal conductivity were made at 100 and 150 psia, from 2000 to 4500°F, following the same procedures used in the hydrogen experiments. The results of these measurements are shown in Fig. 18. At temperatures up to about 3000°F the results are in fair agreement with those reported in Reference 9. Above this temperature, however, the values are higher than those that might be expected from an extrapolation of the existing data. There are no published experimental data with which to compare these values at temperatures above 3000°F.

6.5 CONCLUSIONS

From the exploratory experiments previously described and the preliminary evaluations of simultaneous conduction and radiation heat transfer discussed in Appendix II, the following conclusions have been drawn concerning the feasibility of extending this method of thermal conductivity measurement to other gases:

1. New analytical models which relate gas and effective thermal conductivities and which give the temperature distribution within the specimen must be developed. These new models must consider both conduction and radiation heat fluxes, and must be for a cylindrical geometry.

2. The optical and thermal properties of ceramic materials must be determined in the temperature range of interest. A limited amount of information on these properties exists for a few materials, but no data exist at the temperature range 3000 to 5000°F.

3. A radiating susceptor provides the desired heating at the cylindrical surface of a nonconducting ceramic test specimen.

4. The analytical models and porous tungsten test specimens used in determining hydrogen thermal conductivities result in reasonable thermal conductivity measurements for a gas such as helium whose value of thermal conductivity is of the same order as that of hydrogen.
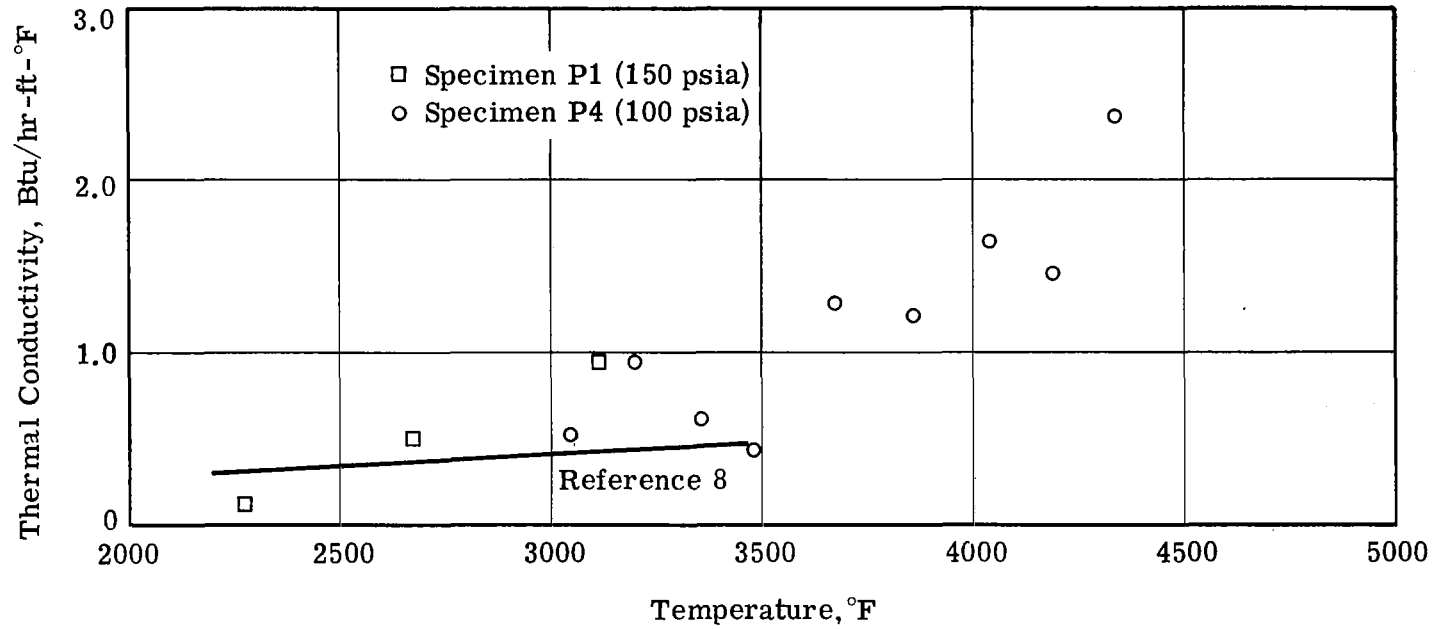
Fig. 18 — Helium Thermal Conductivity

7. APPENDIXES

7.1 APPENDIX I — ANALYSIS OF TRUNCATED-SPHERE MODEL*

7.1.1 Derivation of Effective Conductivity Equation

Because of symmetry and the absence of a particle-size effect, the effective conductivity of a cubic array of truncated spheres may be calculated by considering 1/8 of a particle within a unit cube. Applying unit temperature difference makes the effective conductivity equal to the total rate of heat transfer through the cube. This volume is divided into three regions (I — Solid Conduction, II — Series Conduction, and III — Gas Conduction) as shown in two views in Fig. 19. This figure also shows the differential element of volume used in the integration for the series-conduction region (II).

From the figure it is clear that the radius of contact r is related to the relative contact area δ by

$$\delta = \frac{\pi}{4} r^2$$

and that the radius of the sphere R is

$$R = \sqrt{1 + r^2}$$

---

*Taken from UNC-5082.

Elevation

Plan

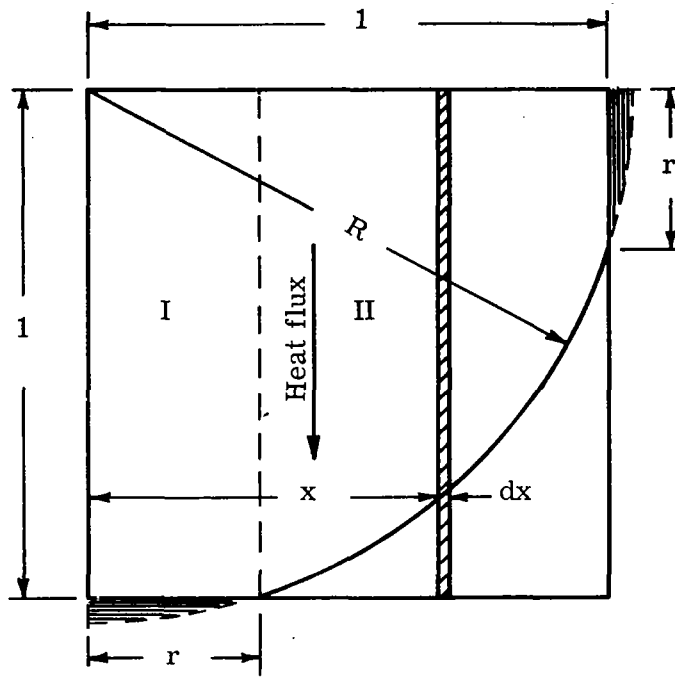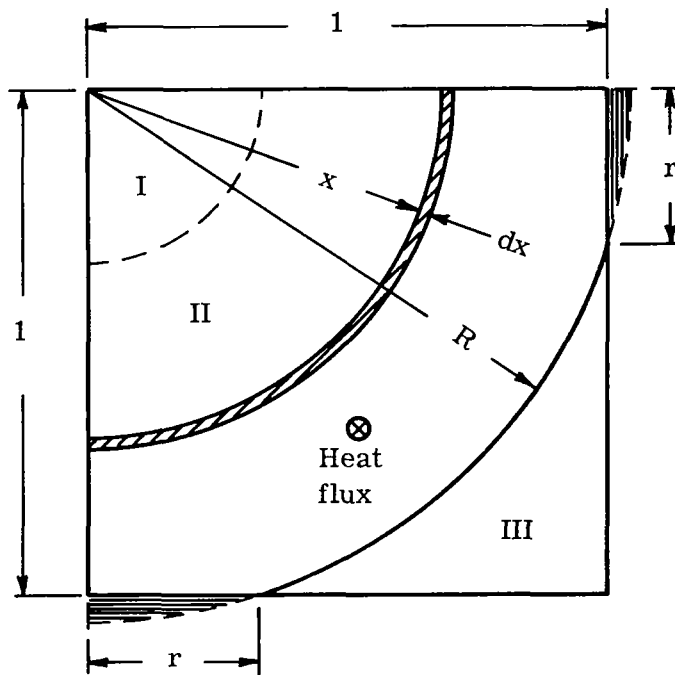Fig. 19 — Unit Cell for Truncated-Sphere Model

Region I — Solid Conduction

$$q_I = \frac{\pi}{4} r^2 k_s = \delta k_s$$

Region II — Series Conduction

$$r < x < 1: dq_{II} = \frac{\pi}{2} k_g \frac{x\,dx}{1 - (1-\beta)\sqrt{R^2 - x^2}}$$

$$1 < x < R: dq_{II} = \left(\frac{\pi}{2} - 2\tan^{-1}\sqrt{x^2 - 1}\right) k_g \frac{x\,dx}{1 - (1-\beta)\sqrt{R^2 - x^2}}$$

$$q_{II} = \frac{\pi}{2} k_g \int_r^1 \frac{x\,dx}{1 - (1-\beta)\sqrt{R^2 - x^2}} + k_g \int_1^R \frac{\left(\frac{\pi}{2} - 2\tan^{-1}\sqrt{x^2-1}\right) x\,dx}{1 - (1-\beta)\sqrt{R^2 - x^2}} \qquad (6)$$

This term can be evaluated with only a slight error by neglecting the quantity $2\tan^{-1}\sqrt{x^2-1}$, i.e., by extending the integration through the shaded region outside the unit cube as though the sphere were not truncated at the side contacts. Because of the three-dimensional geometry, the excess volume included is very small; furthermore, the thickness of the gas layer is greatest in this region, so that the error incurred is very small except for a gas with extremely high conductivity. The heat flux in Region II is then given by the integral

$$q_{II} = \frac{\pi}{2} k_g \int_r^R \frac{x\,dx}{1 - (1-\beta)\sqrt{R^2 - x^2}} \qquad (7)$$

which can be evaluated by making the substitution $u = \sqrt{R^2 - x^2}$ to yield the form

$$q_{II} = \frac{\pi}{2} k_g \int_0^1 \frac{u\,du}{1 - (1-\beta)u} = \frac{\pi}{2} k_g \left[\frac{1}{(1-\beta)^2} \ln\frac{1}{\beta} - \frac{1}{1-\beta}\right] \qquad (8)$$

It is interesting to note that this result is exactly the same as that obtained by Deissler and Eian[5] for the series-conduction region of untruncated spheres. Mathematically, the definite integral (Eq. 7) is independent of the value of R, although it appears in both the integrand and the limits of integration. Physically, this result means that the combined effects of gas-layer thickness and circumference are the same in moving from the contact point to the outer limit for the two cases. Thus, both models show basically the same effect of increasing gas conductivity on the effective conductivity.

Region III — Gas Conduction

$$dq_{III} = k_g \int_1^{\sqrt{2}} \left(\frac{\pi}{2} + 2 \tan^{-1} \sqrt{x^2 - 1}\right) x\,dx$$

This term is small, except when the gas conductivity is extremely high. Rather than evaluate the integral, an approximation is used which compensates exactly for the error incurred in Region II at the limiting condition where $k_g/k_s = 1$, and partially compensates for it at intermediate values of k_g/k_s. This approximation is

$$q_{III} = \left(1 - \frac{\pi}{4} - \delta\right) k_g$$

which is equivalent to subtracting the contact area, δ, from the gas area, $1 - \pi/4$, of the case where $\delta = 0$.

Total Effective Conductivity

Adding the heat fluxes through the three regions, and nondimensionalizing, yields the expression for the effective conductivity of a cubic array of truncated spheres

$$\frac{k_e}{k_s} = \delta + \frac{\pi}{2} \frac{\beta}{(1-\beta)^2} \left[\ln \frac{1}{\beta} - (1-\beta)\right] + \left(1 - \frac{\pi}{4} - \delta\right) \beta \tag{9}$$

7.1.2 Estimation of Error in Calculation of Series-Conduction Term

The series-conduction term given in Eq. 9 is too large by the amount

$$2\beta \int_1^R \frac{(\tan^{-1} \sqrt{x^2 - 1})\, x\, dx}{1 - (1-\beta)\sqrt{R^2 - x^2}}$$

Making the substitution $u = \sqrt{R^2 - x^2}$ and the small-angle approximation $\tan^{-1}\sqrt{x^2 - 1} \approx \sqrt{x^2 - 1}$ yields the form

$$2\beta \int_0^r \frac{\sqrt{r^2 - u^2}\, u\, du}{1 - (1-\beta)u}$$

The maximum value of r for the porous specimens considered is approximately 0.4. Therefore, the range of values of the denominator of the integrand is 0.6 to 1.0 for $\beta = 0$, and less for $\beta > 0$. The magnitude of the error term, which is always small, can be estimated with sufficient accuracy by setting the variable, u, in the denominator equal to its average value, $r/2$, allowing the integral to be evaluated:

$$\frac{2\beta}{1 - (1-\beta)\frac{r}{2}} \int_c^r \sqrt{r^2 - u^2}\, u\, du = \frac{\frac{2}{3}\beta r^3}{1 - (1-\beta)\frac{r}{2}}$$

Evaluation for $r = 0.4$, $\beta = 0.01$

$$\text{Correction term} \quad \frac{\left(\frac{2}{3}\right)(0.01)(0.4)^3}{1 - \frac{(0.99)(0.4)}{2}} = 0.000532$$

Uncorrected value   0.05785

$$\text{Relative error} \quad \frac{0.000532}{0.05785} < 1\%$$

Evaluation for r = 0.4, β = 0.1

$$\text{Correction term } \frac{\left(\frac{2}{3}\right)(0.1)(0.4)^3}{1-\frac{(0.9)(0.4)}{2}} = 0.00521$$

Uncorrected value   0.2722

$$\text{Relative error } \frac{0.00521}{0.2722} < 2\% .$$

At higher values of β, the correction term increases, but it is partly compensated for by the term for Region III; the total error decreases to zero at β = 1.

7.2 APPENDIX II – HEAT TRANSFER BY SIMULTANEOUS CONDUCTION AND RADIATION

7.2.1 Introduction

Some knowledge of heat transfer by simultaneous conduction and radiation is necessary in evaluating the feasibility of extending to other gases the method of measuring thermal conductivity used in this program. The use of highly porous refractory metal and ceramic test specimens introduces significant radiation heat fluxes within the specimen. These radiation heat fluxes must be considered in relation to the conduction heat fluxes to define accurately temperature distributions within the specimen and to relate gas thermal conductivity to the effective thermal conductivity of the test specimen.

The development of analytical models in the proper geometries which accurately describe these simultaneous heat fluxes is beyond the scope of the present program. However, a study has been conducted to provide information for qualitative evaluations.

7.2.2 Background

Recent developments in advanced designs for gas-cooled nuclear reactors for space propulsion, solid-fueled, high power intensity nuclear reactors, hypersonic flight, etc. have aroused interest in heat transfer phenomena at very high temperatures. This new temperature regime brings to the fore considerations of heat transfer by radiation. Heretofore, the relative magnitudes of the heat transfer modes allowed neglect of radiation in the presence of transfer by conduction and convection. In furnaces and combustion chambers where that approach was not possible the solutions have been empirical. The solutions were made with minimal phenomenological theory and, in turn, with neglect of conduction and convection. In those cases where the heat transfer mechanisms were considered simultaneously, they were usually simply added. This is a gross approximation procedure that takes no account of the interactions and nonlinearities of the phenomena.

The equations of conduction and convection are differential equations, usually linearized by assumption of relative constancy of transport properties, boundary layer theories, etc. Radiation problems are usually formulated with integral equations and involve essential nonlinearities due to power functions of the temperature. Simultaneous conduction and radiation processes involve nonlinear integro-differential equations that have been solved for only a few particular cases.

The general approaches to these problems, as discussed by Oppenheim,[10] are the accounting, network, and calculus methods. The first two give net heat fluxes but do not give temperature distributions. Temperature distributions are needed to examine the influence of transport properties and the relative importance of the simultaneous radiative and conductive heat fluxes. A qualitative description of the temperature distributions resulting from combined radiation and conduction heat fluxes within porous materials is given in the following sections.

7.2.3 Simultaneous Radiation and Conduction in an Absorbing Medium

This case is applicable to a high temperature solid through which heat is being transmitted. Even though the absorptivity for radiation may be high, and the thicknesses of solid may be appreciable, the radiation fluxes grow with the fourth power of the absolute temperature and may become even greater than the conduction fluxes. In atomic power fuel elements involving ceramic materials at temperatures near their melting points, radiation fluxes and their interaction with conduction must be considered in calculating temperature distributions.

The results of an analysis by Viskanta and Grosh[11] demonstrate these interactions. The analysis assumed an isotropic, homogeneous medium at rest, which absorbed and emitted thermal radiation. The thermal conductivity and absorption coefficient were assumed to be constant. A one-dimensional geometry, such as the space between two parallel infinite planes, was assumed, and the system was considered to be at a steady state.

Using the above assumptions, the following expression was derived for the heat transfer through a slab of thickness, x.

$$q'' = \frac{k}{x} (T_x - T_0) + 2 \left\{ \rho(0) \left[(1-\epsilon_T) E_3(\tau_0) + \frac{1}{\tau_0} E_4(\tau_0) - \frac{1}{3\tau_0} \right] + \right.$$

$$+ \rho(\tau_0) \left[-\frac{1}{\tau_0} E_4(\tau_0) - \frac{1}{2} + \frac{1}{3\tau_0} \right] + \frac{\epsilon_T}{2} \sigma T_x^4 +$$

$$+ \sigma \int_0^{\tau_0} n^2 [(1 - \epsilon_T) E_2(\tau_0 - \tau')] +$$

$$+ \frac{1}{\tau_0} [E_3(\tau_0 - \tau') - F_3(\tau')] T^4 \, d\,\tau' \left. \right\} \tag{10}$$

A rigorous solution of this relatively simple energy equation is seen to be extremely difficult. It is evident from an inspection of the expression, however,

that the presence of thermal radiation changes the temperature distribution by the introduction of fourth-power temperature terms. It is also evident that the heat flux due to conduction is augmented by these radiation terms. The optical and thermal properties of the material determine the amount of radiation heat flux added and the degree to which the temperature distribution is affected. Klein[12] presents qualitative descriptions of how the effective thermal conductivity of a porous material is affected by these internal radiation heat fluxes.

Using a model of many parallel infinite layers for the porous material, he describes the two cases shown in Fig. 20. The illustrations show typical temperature distributions and the points of origin and absorption of the radiation rays for a large optical thickness material and for an intermediate optical thickness material.

The large optical thickness material is characterized by negligible surface effects, i.e., radiation does not penetrate the surface of the solid material. Since these surface effects are negligible, the temperature drop across the solid is a function of the amount of solid, and increasing the number of spaces by making the layers thinner (while keeping the same porosity) will not change the total temperature drop across the solid. However, it will increase the number of spaces. Since these spaces are thermal resistances, increasing the number of pores will decrease the effective thermal conductivity. The effect is analogous to that of using radiation shields in a given distance to decrease radiant heat losses. If enough shields are included, radiation losses are essentially eliminated. This was observed to be the case for the porous tungsten specimens used in the hydrogen measurements.

Intermediate optical thickness materials represent the most important case in evaluating the feasibility of extending this method of gas thermal conductivity measurement to other gases. Most ceramic materials fall in this intermediate

Temperature

Radiation paths

Large optical thickness

Temperature

Radiation paths

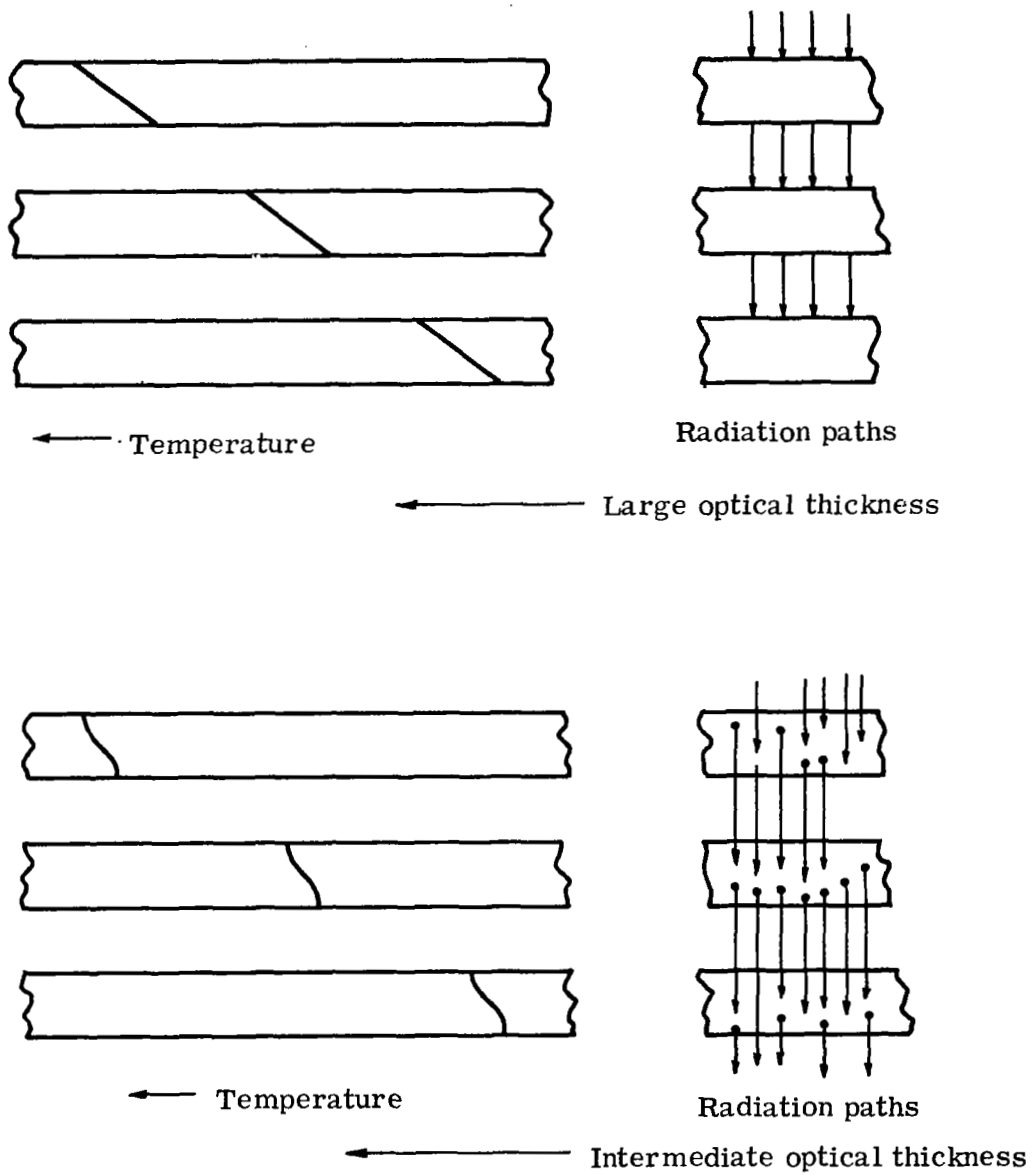Intermediate optical thickness

Fig. 20 — Heat Transfer Through Layers

optical range. The effective thermal conductivities of these porous ceramic materials still depend on the thickness of the layers and number of spaces. However, surface effects are no longer negligible and significant amounts of radiation penetrate the surfaces and are absorbed within the solid ceramic material, resulting in nonlinear temperature distributions within the material. This condition is of importance in establishing the desired value for the effective thermal conductivity of a porous ceramic specimen. As particle size decreases, expected decreases in the effective thermal conductivity are offset by the decreased optical thickness which allows radiation to pass through the structure.

7.2.4 Simultaneous Radiation and Conduction in an Absorbing and Scattering Medium

In addition to the radiation and conduction heat transfer mechanisms in an absorbing material, gray, porous materials introduce a scattering mechanism for transferring the radiant energy. An analysis by Viskanta[13] resulted in the following expression for the temperature distribution in a flat slab, gray body, porous radiating material

$$\frac{d^2\theta}{d\tau^2} = N\ (1 - \omega_0)\left[\theta^4(\tau) - \frac{1}{4}\ \zeta\ (\tau)\right] \tag{11}$$

If radiation is absent, $N = 0$. If the media does not absorb, but only scatters, $\omega_0 = 1.0$, the temperature varies linearly from one surface to the other. For these conditions the conduction heat transfer is independent of radiation and the total heat transfer is additive for the two modes. However, porous ceramic materials may be expected to absorb and to scatter radiation energy, and a nonlinear distribution will result.

7.2.5 Conclusions

The above discussions indicate that an accurate understanding of the relation between simultaneous radiation and conduction heat transfer requires a knowledge

of the optical and thermal properties of the materials at the temperatures of interest. Chen and Churchill[14] have made measurements of the scattering and absorption coefficients of isothermal beds of spheres of glass, aluminum oxide, steel, and silicon carbide at temperatures from 800 to 2000°F. Klein[12] has measured absorption and scattering coefficients for powdered zirconia at temperatures up to 3000°F. The results of these measurements indicate that scattering is a major mechanism for the attenuation of radiation, and that the value of the scattering coefficient is a strong function of particle size. For example, Chen and Churchill report a scattering coefficient of 350 ft^{-1} for polished carbon steel spheres, 1/8-in. to 3/10-in. in diameter. Klein reports values 10 times greater for the scattering coefficients of powdered zirconia of particle sizes 0.003 to 0.020 mils in diameter.

No known measurements of the optical properties of any material above 3000°F exist.

8. NOMENCLATURE

a	Fractional cross section of gas phase
h_{rp}	Equivalent heat-transfer coefficient, pore-to-pore radiation
h_{rs}	Equivalent heat-transfer coefficient, surface-to-surface radiation
k	Thermal conductivity
ℓ	Length of conduction path
L	Half-length of porous specimen
Q_{nc}	Heat flux to convection
r	Radial coordinate
R	Radius to inner edge of heated layer
S_0	Proportionality factor
T	Absolute temperature
z	Axial coordinate
β	Ratio of gas thermal conductivity to solid thermal conductivity
δ	Fractional contact area of solid phase
ϵ_T	Total hemispherical emittance
ϵ_λ	Spectral emittance
σ	Stefan-Boltzmann radiation constant
φ	Relative length of conduction path
q''	Heat transfer per unit area
ρ	Radiosity, radiant energy leaving a surface
E	Net radiative emission per unit volume

τ Optical thickness

n   Refractive index

θ Dimensionless temperature

N   Ratio of conductive to radiative heat fluxes

ω_0 Albedo for single scattering

$\zeta(\tau)$ Dimensionless incident radiation

Subscripts

e   Effective

g   Gas phase

0   Center

s   Solid phase

9. REFERENCES

1. Grier, N.: Calculation of Transport Properties and Heat Transfer Parameters of Dissociating Hydrogen, NASA TN-D-1406.

2. Hoch, M. and Nitti, D.: New Method for the Determination of Thermal Conductivities between 1000° and 3000°C, ASD-TR 61-528 (June 1962).

3. Yagi, S and Knuii, D.: Studies on Effective Thermal Conductivities in Packed Beds, J. Am. Inst. Chem. Eng., 3:3 (Mar. 1957).

4. Kunii, D. and Smith, J.: Heat Transfer Characteristics of Porous Rocks, Am. Inst. Chem. Eng., 6:1 (Mar. 1960).

5. Deissler, R. and Eian, C.: Investigation of Effective Thermal Conductivities of Powders, NACA RM E52C05 (June 1952).

6. Gorring, R. and Churchill, S.: Thermal Conductivity of Heterogeneous Materials, Chem. Eng. Prog., 57:7 (July 1961).

7. Israel, S., Hawkins, T., and Hyman, S.: Thermal Properties of Solid and Porous Tungsten at Temperatures to 5000°F, UNC-5127, NASA CR number pending (Aug. 1965).

8. Israel, S., Hawkins, T., and Hyman, S.: Experimental Data for the Effective Thermal Conductivity of Solid and Porous Tungsten in Vacuum and Hydrogen Atmospheres, NASA-CR-54429 (Aug. 1965).

9. Mann, J. and Blais, N.: Thermal Conductivity of Helium and Hydrogen at High Temperatures, LA-2316 (Sept. 1959).

10. Oppenheim, A. K.: The Engineering Radiation Problem — An Example of the Interaction Between Engineering and Mathematics, Zeit. fur Avg. Math and Mech., 36:81-93 (1956).

11. Viskanta, R. and Grosh, R. J.: Heat Transfer by Simultaneous Conduction and Radiation in an Absorbing Medium, pp. 63-72, J. of Heat Trans.(Feb. 1962).

12. Klein, J. D.: Heat Transfer by Radiation in Powders, Ph.D. Thesis, MIT (June 1960).

13. Viskanta, R.: Heat Transfer by Conduction and Radiation in Absorbing and Scattering Materials, Paper No. 64-HT-33, Presented at ASME Heat Transfer Conference, Cleveland, Ohio, August 1964.

14. Chen, J. and Churchill, S. W.: Radiant Heat Transfer in Packed Beds, J. Am. Chem. Eng., 9:35 (1963).